Equivalent-crystal theory of metal and semiconductor surfaces and defects

John R. Smith and Tom Perry
Physics Department, General Motors Research Laboratories, Warren, Michigan 48090-9055

Amitava Banerjea
National Aeronautics and Space Administration, Lewis Research Center, Cleveland, Ohio 44135 and Physics Department, Kent State University, Kent, Ohio 44242

John Ferrante
National Aeronautics and Space Administration, Lewis Research Center, Cleveland, Ohio 44135

Guillermo Bozzolo
National Aeronautics and Space Administration, Lewis Research Center, Cleveland, Ohio 44135 and Analex Corporation, 21775 Brookpark Rd., Fairview Park, Ohio 44126
(Received 7 January 1991)

A method is proposed for computing material defect and surface properties accurately at the atomic level. The method is both simple and accurate and treats both semiconductors and metals. Lattice defect and surface energies are determined via perturbation theory on a crystal whose lattice constant is chosen to minimize the perturbation. The energy of the equivalent crystal as a function of its lattice constant is given by a universal energy relation. This simple method is tested via predictions of surface energies, surface reconstructions, and bulk distortions of metals and semiconductors. Good agreement is obtained with the results of both experiment and first-principles calculations.

I. INTRODUCTION

This is an exciting period for the theory of solids, because physicists and materials scientists are developing tools to treat real material surfaces and defects at the atomic level, and are having some initial successes in a variety of applications. A number of examples can be found in Ref. 1. Perhaps the most widely used technique is the embedded-atom method of Daw and Baskes.[2,3] The goal is to go well beyond pair potentials and to in fact obtain quantum-mechanical accuracy, and yet to have a method that is simple enough to apply that phenomena such as friction and wear and crack propagation can be computed atomistically.

In the following we describe a method[4–7] which is simple to apply and yet is accurate. It is based on an exact relationship between the total energy and atomic locations and applies to surfaces and defects in both simple and transition metals as well as in covalent solids. This is the first time, to our knowledge, that a single method is shown to treat both metals and covalent solids accurately. Not only does this have practical advantages because many material combinations involve both types of solids, but also the differences and similarities of the types of materials are better understood when they are all treated by a single method. The exact framework is also essential in order to improve accuracy in a systematic fashion and to know what kind of accuracies to expect in applications.

To exemplify the accuracy of the method we will show that predicted surface energies of a variety of fcc and bcc metal surfaces are found on average to be within 10% of first-principles values, yet they can easily be determined with a hand calculator. Predicted changes in interlayer spacings due to surface relaxation of the low index surfaces of Cu, Ni, Al, and Ag will be shown to be typically within experimental error bars, often within 0.01 Å. Predicted (1×1) to (2×1) reconstruction energies and interatomic spacings for Si(100) are found to be in good agreement with first-principles results and with available experiments. While 14 independent atomic coordinates per surface unit cell (spread over five atomic layers) were varied simultaneously to minimize the total energy in the reconstruction, the calculation was nevertheless conveniently carried out on a personal computer.

In this paper we consider only energies and atomic locations associated with surfaces and defects in elemental solids. Work is in progress to extend the method to alloys and solids containing impurities.

In Secs. II A–II D we give the basic idea of the method, including the mathematical formulation. In Secs. II E 1–II E 3 we discuss approximations which simplify the applications. We then give some numerical tips in Sec. II E 4 on how to use the method most easily. In Sec. II E 5 we provide analytical expressions for constants of the method. To aid in applications of the method, we gather the working equations together in Sec. II F. Section III is devoted to results of applications to metals and silicon. This not only exhibits accuracies, but also shows what terms and physical effects are more important for the different classes of solids. A summary of the method can be found in Sec. IV.

II. EQUIVALENT-CRYSTAL THEORY

A. Basic idea

Consider a localized structural defect in a solid such as the vacancy shown in the upper diagram of Fig. 1. We

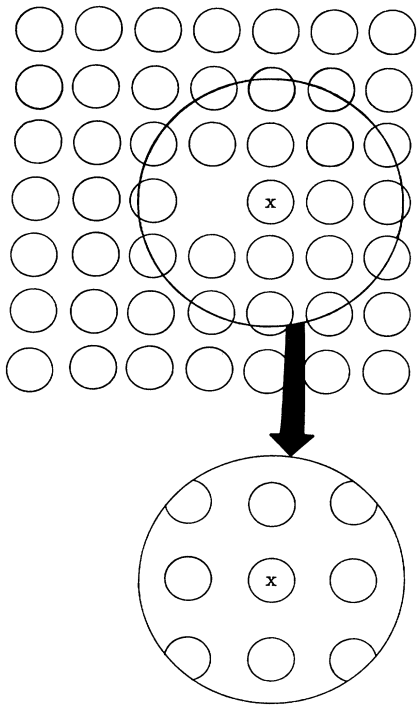

FIG. 1. A vacancy in a two-dimensional square lattice as an example crystal defect. A vacancy nearest neighbor is indicated by an ×. The local environment of the vacancy nearest neighbor is indicated by the circular area. An equivalent-crystal representation of that environment is depicted in the lower circular diagram. The equivalent crystal has the same structure as the crystal containing the vacancy, but the equivalent-crystal lattice constant is somewhat larger since the atom indicated by the × is missing a neighbor. The actual lattice constant is determined by Eq. (3) so that perturbation series vanishes.

would like to compute the energy to form that defect in the single crystal. There are many examples of localized defects in solids. There are point defects like vacancies and interstitials, line defects like dislocations, and planar "defects" like surfaces and interfaces.

The local defect represents a substantial increase in complexity relative to single crystals, and so theorists in modeling surfaces and defects have attempted to retain single-crystal simplicity on a local level. The local-density approximation[8] (LDA) of density-functional theory has been valuable not only in carrying out calculations for crystalline solids, but also for local defects and surfaces. In the LDA the electronic exchange-correlation potential at a particular point in space is assumed to be that of a uniform, free-electron gas whose electron density is the same as the actual electron density evaluated at the same point. The free-electron gas is the simplest single crystal and, in a sense, the LDA assumes that each point in space is represented by such a single crystal. Each different point is represented by a different single crystal, i.e., the constant electron density (or lattice constant) of the single crystal is different for each point represented. One might think this to be a drastic approximation, but in fact the LDA has served well even for solid-vacuum interfaces (see, e.g., Ref. 4), where the electron density variation deviates quite rapidly from that of a uniform, free-electron gas. A second example of a theory based on the framework of single-crystal simplicity on a local level is found in effective-medium theory[9] (EMT). In EMT, the interaction energy of atoms in a solid is found first by computing the electron density provided by atoms surrounding a given atom, and then taking the embedding energy of that atom in the actual solid to be in lowest order the embedding energy in a uniform, free-electron gas of that same electron density. Again, the EMT has been successfully applied even at solid surfaces.

We also retain single-crystal simplicity on a local level in modeling surfaces and defects, but since we are interested in transition metals and covalent solids like semiconductors, which are not free-electron materials, we choose not to rely on a free-electron gas. Rather, we introduce an effective single crystal locally, which differs from the actual ground-state single crystal only in that its lattice constant may be different from the ground-state value. Consider M atoms encompassing the range of the local defect (indicated schematically by atoms within or near the circular area in the upper diagram of Fig. 1). We first replace those M atoms with M atoms of an effective crystal whose lattice constant a is yet to be specified. Next we compute the energy to form the defect or surface via perturbation theory, where the perturbation arises from the difference in the ion core electronic potentials of the actual defect solid or surface and those of the effective bulk single crystal. Let ε be the total energy to form the defect or surface, $E_c(a)$ the total energy per atom of the effective bulk single crystal, and $ME_p(a)$ the sum of the perturbation series:

$$\varepsilon = M[E_c(a) + E_p(a) - E_c(a_m)] , \tag{1}$$

where a_m is the equilibrium lattice constant (minimum in Fig. 2).

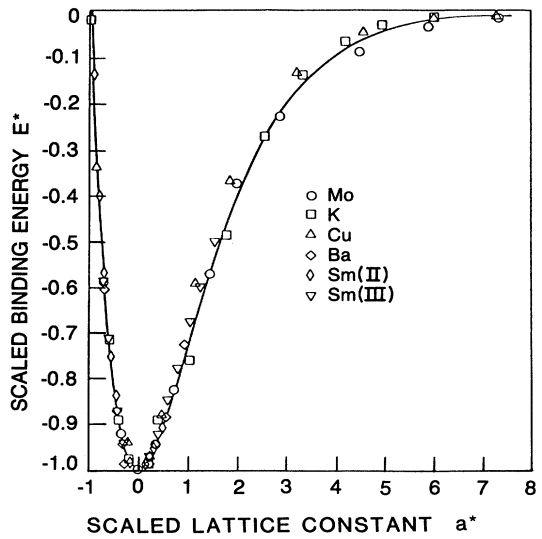

FIG. 2. Scaled cohesive energy E^* per atom of a crystal plotted against interatomic separation a^* for representative solids. The solid line is a plot of the Rydberg function. The sources of the unscaled results are listed in Ref. 12.

The rate of convergence of the perturbation series is important because typically it is difficult to evaluate high-order perturbation terms. Thus it would be desirable to adjust the lattice constant a of the effective crystal so that the perturbation is minimized and thereby hopefully the perturbation series is rapidly convergent. Now if the crystal structure of the actual single crystal is that of the lowest-energy phase, and if its lattice constant is at the ground-state value a_m, then we know that forming the defect or surface must raise the energy of the system above the minimum in the cohesive energy curve. Thus there must be a value a of the lattice constant of the effective crystal such that

$$\varepsilon = M[E_c(a) - E_c(a_m)] , \tag{2}$$

so that

$$E_p(a) = 0 . \tag{3}$$

Since the excitation energy of the effective crystal relative to the ground-state crystal is equal to the total energy to form the local defect or surface [Eq. (2)], we call the crystal of lattice constant a an *equivalent crystal.* Note that we have not only minimized the perturbation series, we have been able to make it sum to zero. Further, while a defect or surface in a solid is a complicated many-atom and many-electron problem, it has now been reduced formally to the solution of one equation, Eq. (3), for the one unknown a. Once a is known, then the energy of the solid containing a surface or defect can be immediately found from Eq. (2), since $E_c(a)$ is known for many single crystals.

Whether this is merely a formal simplification of the defect problem or is in fact a simplification in practice will depend on how difficult Eqs. (2) and (3) are to solve. Let us first consider some practical matters associated with Eqs. (2) and (3).

B. Practical matters

First, one can see from Fig. 2 that there can be two values of a which satisfy Eq. (2) for a given ε. The apparent ambiguity is removed by Eq. (3), however. For surfaces and defects involving missing atoms such as vacancies, the root for $a > a_m$ satisfies Eq. (3). For defects involving compressions like interstitials, the root for $a < a_m$ satisfies Eq. (3). This is perhaps more intuitively obvious if one realizes that Eq. (3) requires the equivalent crystal to mimic accurately the environment in the vicinity of the surface or defect. Making a vacancy effectively lowers the atom density, hence $a > a_m$. Conversely, an interstitial effectively increases the atom density, hence $a < a_m$.

Second, difference energy calculations are notoriously difficult. If one were to attempt to evaluate Eq. (2) straightforwardly, one would be trying to find a relatively small difference between large numbers because M usually is taken to be a relatively large number. This can place impractical requirements on the required accuracy of the large numbers $ME_c(a)$ and $ME_c(a_m)$ in order to obtain a reasonably accurate ε. The change in energy of an atom in the solid near the surface or defect due to surface or defect formation can be a significant fraction of that atom's contribution to the cohesive energy, however. Thus one can circumvent this difficulty by finding the energy change on an atom-by-atom basis. That is, one can find an equivalent-crystal lattice constant $a(i)$ with corresponding energy change ε_i by solving Eqs. (2) and (3) for each atom i near the surface or defect. If

$$\varepsilon_i \equiv E_c(a(i)) - E_c(a_m) , \tag{4}$$

then

$$\varepsilon = \sum_i \varepsilon_i . \tag{5}$$

For an atom i close to the surface or defect, ε_i can be a significant fraction of both $E_c(a(i))$ and $E_c(a_m)$. Thus forming an equivalent crystal for each atom can allow one to extract an accurate energy ε without the need for extremely accurate total-energy calculations.

An equivalent crystal for a particular atom is exemplified by Fig. 1. A nearest-neighbor atom to the vacancy is indicated by an x in both the upper and lower diagrams of Fig. 1. In the upper diagram of Fig. 1 we have the actual atomic array, while in the lower diagram we see the equivalent-crystal atoms associated with atom x. Note that the lattice constant of the equivalent crystal is a little larger than that of the actual crystal because atom x is next to a vacancy, as discussed above.

Note also that the solution of Eqs. (2) and (3) for atom i does not depend on the solution for any other atom j. Thus computational time only depends linearly on N, where N is the total number of atoms whose energy is changed significantly by the introduction of the surface or defect. This is a great simplification. Moreover, in practice we have found for metals and covalent semiconductors that only a few neighbors contribute significantly to Eq. (5). For example, for metal surfaces, typically only the surface atomic layer and the atomic layer beneath it need be included. For Si(100) reconstruction we included the top five atomic layers, still a relatively trivial computational requirement for this method.

C. Universal energy relation

Let us first consider the function $E_c(a)$. There is a simple, universal form for $E_c(a)$. In fact it has been discovered[10–12] that total energies as a function of interatomic spacings have a single, universal form for bimetallic adhesion, for cohesion in metals, for metallic and covalent bonds in chemisorption, for many diatomic molecules, and even nuclear matter. This is exemplified in Figs. 2 and 3. In Fig. 2 we find cohesion results for a variety of metals, and in Fig. 3 typical curves for cohesion, adhesion, chemisorption, and diatomic energetics. All of these curves are scaled on to one universal form. The universal form can be obtained by a simple scaling of the total energy:

$$E^* = E(a)/\Delta E , \tag{6}$$

where

$$a^* = (a - a_m)/l , \tag{7}$$

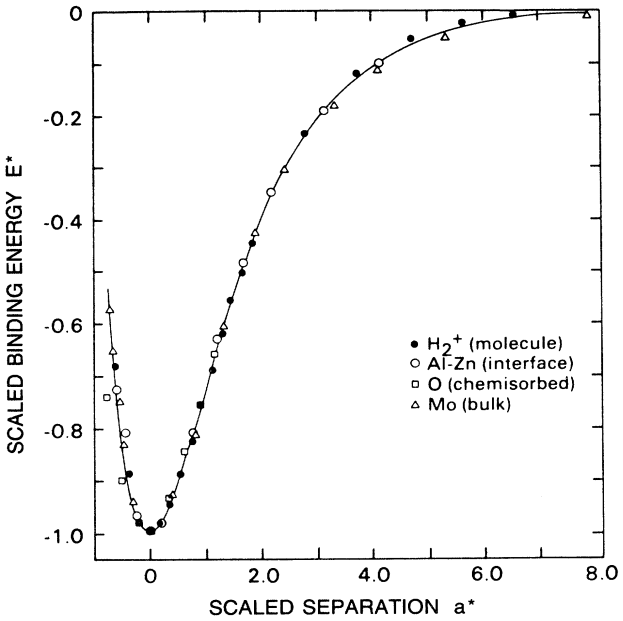

FIG. 3. Scaled binding energy E^* plotted against the scaled separation a^* for representative cases of cohesion, bimetallic adhesion, chemisorption, and a diatomic molecule. The solid line is a plot of the Rydberg function. The sources of the unscaled results are listed in Ref. 12.

and ΔE is the minimum value of the total energy, i.e., the equilibrium binding energy. The scaling length l is defined for convenience so that $[d^2E^*(a^*)/da^{*2}]_0=1$ for all scaled curves:

$$l=\sqrt{\Delta E/[d^2E(a)/da^2]_{a=m}} \ . \tag{8}$$

For the cohesion curves $E_c(a)$ [which we need for Eqs. (2) and (3)], we take $a=r_{\rm WS}$, where $r_{\rm WS}$ is the Wigner-Seitz radius of equilibrium value $r_{\rm WSE}$, so that

$$a^*=(r_{\rm WS}-r_{\rm WSE})/l \tag{9}$$

and

$$l=\sqrt{\Delta E/12\pi Br_{\rm WSE}} \tag{10}$$

for cohesion, where B is the equilibrium bulk modulus and ΔE is the cohesive energy. There is in fact a simple analytic form which accurately represents the universal energy relation:

$$E^*(a^*)=-(1+a^*)e^{-a^*} \ . \tag{11}$$

This analytic form is the solid line plotted in Figs. 2 and 3. We find then that

$$E_c(a)=-\Delta E(1+a^*)e^{-a^*} \tag{12}$$

and

$$\varepsilon_i=-\Delta E\,F^*[a^*(i)] \ , \tag{13}$$

where

$$\begin{aligned}F^*[a^*(i)]&=1+E^*[a^*(i)]\\&=1-[1+a^*(i)]e^{-a^*(i)} \ .\end{aligned} \tag{14}$$

Knowing that there is a universal energy relation and being able to represent it by a simple, analytic form gives us a good start on the surface or defect problem.

In fact, a number of other methods also rely on the universal nature[11] of the cohesive energy relation in different ways. For metals Daw and Baskes[2,13] employ the universal energy relation in their widely-used embedded-atom method (see also Ref. 14). The universal energy relation is also found in the semiconductor methods of Tersoff,[15] Baskes, Nelson, and Wright,[16] and Dodson.[17]

D. Formal perturbation series

Next we concentrate on the sum of the perturbation series, $E_p(a(i))$, associated with the equivalent crystal for atom i [see Eq. (1) and the discussion associated with Eq. (5)]. First we will display it formally, and then we will seek accurate approximations to it consistent with our goal of providing a method for treating real material surfaces and defects at the atomic level. Figure 1 may be helpful in visualizing the equivalent crystal and actual environments for atom i. In that example, atom i is taken to be a nearest neighbor to a vacancy indicated by an x in both the upper and lower diagrams as mentioned earlier. For a general local defect or surface we have

$$\begin{aligned}E_p[a(i)]=&\int_{V_i}d\mathbf{r}\,\delta v(\mathbf{r})[n(\mathbf{r})-Z\delta(\mathbf{r}-\mathbf{R}_i')]\\&+E_2+E_3+\cdots \ .\end{aligned} \tag{15}$$

Here V_i is the unit-cell volume containing atom i in the equivalent crystal, $n(\mathbf{r})$ is the valence-electron electron density distribution in the equivalent crystal, Z is the valence, $\delta v(\mathbf{r})$ is the change in ion-core potential when the actual solid is replaced by the equivalent crystal;

$$\delta v(\mathbf{r})=\sum_m[v(\mathbf{r}-\mathbf{R}_m')-v(\mathbf{r}-\mathbf{R}_m)] \ , \tag{16}$$

$\mathbf{R}_m$ is a set of position vectors of the equivalent crystal, $\mathbf{R}_m'$ that of the actual solid containing a local defect ($\mathbf{R}_i=\mathbf{R}_i'$), the first-order perturbation term is

$$E_1=\int_{V_i}d\mathbf{r}\,\delta v(\mathbf{r})[n(\mathbf{r})-Z\delta(\mathbf{r}-\mathbf{R}_i')] \ , \tag{17}$$

and E_2 is second order in the perturbation $\delta v(\mathbf{R})$;

$$E_2=\tfrac{1}{2}\int_{V_i}d\mathbf{r}\,\delta n(\mathbf{r})\delta v(\mathbf{r}) \ , \tag{18}$$

where

$$\delta n(\mathbf{r})=\int d\mathbf{r}'\,L(\mathbf{r},\mathbf{r}')\delta v(\mathbf{r}') \tag{19}$$

and $L(\mathbf{r},\mathbf{r}')$ is the linear-response function of the equivalent crystal.

Equations (15)–(19) call for a few comments. First, one can see from Eq. (16) that $\delta v(\mathbf{r})$ derives from a neutral charge distribution, as does the quantity in square brackets in Eq. (15) and $\delta n(\mathbf{r})$ in Eqs. (18) and (19). This limits the range required to only a few neighbors of atom i, thereby simplifying the evaluation of $E_p(a(i))$. Second, note that in general $\delta n(\mathbf{r})$ has the effect of screening $\delta v(\mathbf{r})$. This is a nontrivial effect which we will want to in-

clude in our calculations. Finally, an exact evaluation of the perturbation series would be too time consuming for our goal of treating real material surfaces and defects. Thus we look for accurate approximations in the next section.

E. Approximations to the perturbation series

1. Derivations and discussion of the standard form

The formal perturbation series is instructive as to the form and type of approximations needed. For ease of calculation we have approximated it by simple, analytic forms which contain a few parameters. These parameters can be evaluated from experimental results or from the results of first-principles calculations. We follow the spirit of pseudopotential perturbation techniques in simple metals[18] and transition metals.[19,20] Those methods yielded a perturbative series, the first term of which has been called a "volume" term, i.e., a term which is a function of the number of atoms per unit volume. Successively-higher-order perturbation terms contain successively-higher-order many-atom interactions. Our perturbation series contains a term analogous to the volume term, plus two-, three-, and four-body terms. In this section we will provide discussion and derivations of the standard form of the method. In Secs. II E 2 and II E 3 we will present simpler and more general forms of the method, respectively. Later we will discuss some details of how best to use the method, and finally we will present the results of a number of applications.

Our simplified perturbation series for ε_i is of the form

$$\varepsilon_i = \Delta E \left[F^*[a_1^*(i)] + \sum_j F^*[a_2^*(i,j)] + \sum_{j,k} F^*[a_3^*(i,j,k)] + \sum_{p,q} F^*[a_4^*(i,p,q)] \right] . \tag{20}$$

F^* is the simple analytic function discussed earlier:

$$F^*[a^*] = 1 - (1 + a^*)e^{-a^*} , \tag{21}$$

and the scaled lattice constants a^* are given in terms of the equivalent-crystal nearest-neighbor distances R_{ec} as [see Eq. (9)]

$$a^* = (R_{ec}/c - r_{WSE})/l , \tag{22}$$

where $c = \sqrt{2}(2\pi/3)^{1/3}$ for fcc, $c = (\sqrt{3}\pi)^{1/3}$ for bcc, and $c = (\sqrt{3}\pi/2)^{1/3}$ for diamond structures.

The first term in Eq. (20), $F^*[a_1^*(i)]$, contributes when average neighbor distances are altered via defect or surface formation. It can be thought of as representing local atom density changes. There is some similarity between this term and a localized version of the "volume" term found in perturbation theory of nearly free electron and transition metals.[18–20] For an isotropic volume deformation, as exemplified in Fig. 4(b) for the diamond structure (see Fig. 5 for other structures), the only term contributing in Eq. (20) to ε_i is $F^*[a_1^*(i)]$. In fact, in that case this term gives ε_i to the accuracy of the universal energy relation [see Eq. (14)].

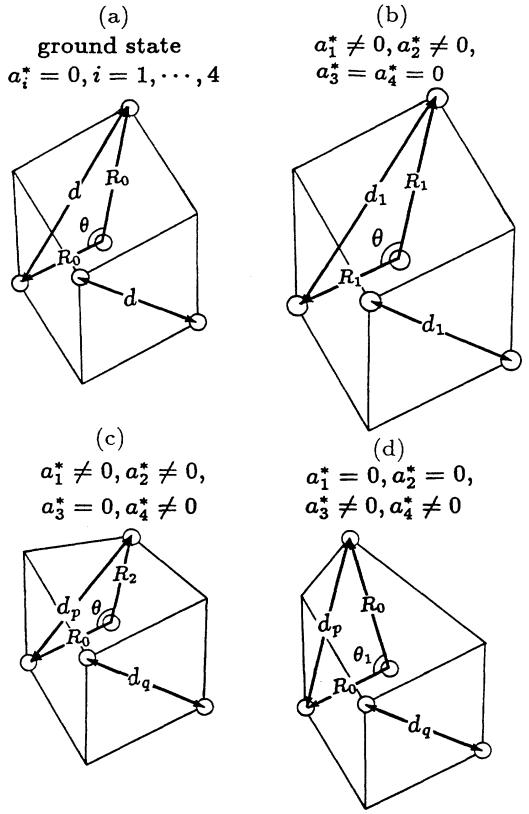

FIG. 4. In this figure we use the diamond structure to illustrate the types of lattice distortions that might be encountered. General distortions are a combination of those shown. In (a), the ground-state structure is given, with all three equivalent-crystal lattice constants being zero by definition. In (b), an isotropic distortion is illustrated, where all nearest-neighbor bond lengths have increased from R_0 to R_1. Since bond lengths have increased, $a_1^* > 0$. Since all bond lengths are equal, $a_2^* = 0$, since there is no bond-angle change, $a_3^* = 0$, and since the face diagonals are equal, $a_4^* = 0$. In (c) one bond length has decreased, while no bond-angle change occurs. Thus a_1^*, a_2^*, and a_3^* deviate from zero, while a_3^* remains zero. Finally, in (d) all bond lengths remain equal to R_0 ($a_1^* = 0$, $a_2^* = 0$), but bond angles and face diagonals distort ($a_3^* \neq 0$ and $a_4^* \neq 0$).

For anisotropic deformations, however, ε_i clearly will depend on more than a term like $F^*[a_1^*(i)]$ which is a functional of only average distances. The three other terms in Eq. (20) contribute for anisotropic distortions. They are obtained, as described below [following Eq. (27)], by the consideration of anisotropy energies arranged in the order of numbers of atoms involved. $F^*[a_2^*(i,j)]$ is a two-atom term, $F^*[a_3^*(i,j,k)]$ is a three-atom term, and $F^*[a_4^*(i,p,q)]$ is a four-atom term. We found that one did not need to go beyond the four-atom term to obtain accurate results.

We treat the several different terms in the perturbation series as linearly independent, so that each term satisfies

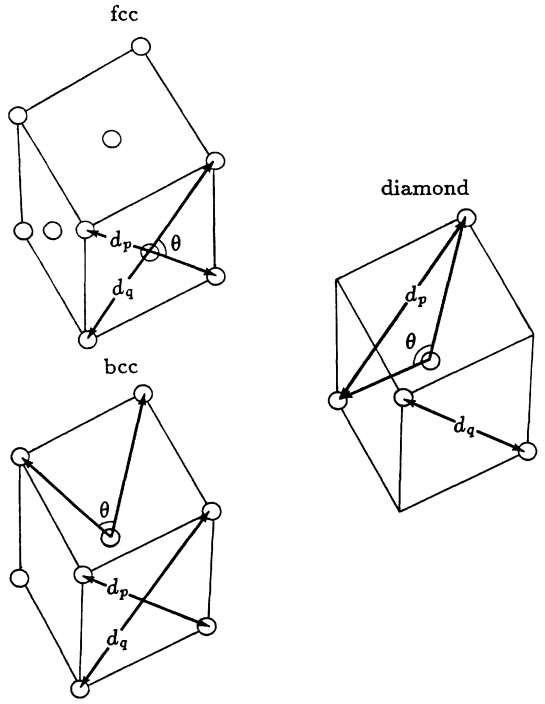

FIG. 5. Crystal structures for face-centered, body-centered, and diamond structures.

Eq. (3) for the corresponding equivalent-crystal lattice constant. Linear independence is consistent with the limit of small perturbations, which in turn is consistent with the spirit in which we present equivalent-crystal theory. We will see that we can successfully apply it to surfaces where the perturbation would seem not to be small. This is due in part because we choose the equivalent-crystal lattice constant to make the perturbation equal to zero in every case.

Equation (20) appears to be more complicated than Eq. (2) because there are now several terms and several equivalent-crystal lattice constants, while Eq. (2) has only one. We will see however that solving for the equivalent-crystal lattice constants $a_1^*(i)$, $a_2^*(i)$, $a_3^*(i,j,k)$, and $a_4^*(i,p,q)$ is relatively trivial, and they are all we need to know to simply evaluate the total energy via Eqs. (20) and (21). This is an enormous simplification over attempting a frontal assault on Eqs. (3) and (15).

The energy terms of Eq. (20) are based on the framework provided by the formal perturbation series and a physically intuitive division of the defect or surface formation energy into three categories or terms. The first term is a many-atom term which is insensitive to bond-angle or bond-length anisotropies. The form of the perturbation terms leading to $F^*[a_1^*(i)]$ is based on the first- and second-order perturbation terms of Eqs. (15)–(19). The perturbation, as mentioned earlier, is due to the difference in potentials between a solid containing a defect or a surface and the bulk ground-state single crystal. Consider the first-order term, which is the first term on the right-hand side of Eq. (15). Its variations with R, the variation of interest, is determined primarily by the behavior in the overlap region. This is the region in which the electron density of an atom overlaps the potential $v(\mathbf{r}-\mathbf{R})$ of a neighboring atom. Strictly speaking, the unperturbed electron density we should be talking about is the electron density $n(\mathbf{r})$ of the equivalent-crystal unit cell, rather than an atomic density. One can always represent a crystalline electron density $n(\mathbf{r})$ as a sum of identical, overlapping functions $n_A(\mathbf{r}-\mathbf{R}_m)$, localized about the equivalent-crystal lattice sites $\mathbf{R}_m$:

$$n(\mathbf{r})=\sum_m n_A(\mathbf{r}-\mathbf{R}_m)\ . \tag{23}$$

In the overlap region, we encounter the tails of the functions $n_A(\mathbf{r}-\mathbf{R}_m)$. Let us approximate the functions in this overlap region as having the form of the electron density of the highest partially occupied atomic level of the atoms making up the crystal. We know that in the atom, this is the level which will dominate the long-range behavior, and so may be representative of the tail region. Further, one might presume that the atomic core is relatively small, and hence that $v(\mathbf{r}-\mathbf{R})$ is relatively well localized about $\mathbf{R}$. Then the dependence of E_1+E_2 [Eqs. (17) and (18)], on R would mimic the form of the electron density of the highest partially occupied atomic level, i.e.,

$$E_1+E_2 \propto R^p e^{-\alpha R} \tag{24}$$

for nearest neighbors, where $p=2n-2$ and n is the atom principal quantum number. We must keep in mind that the second-order perturbation is the first term in the series to involve electronic screening, $\delta n(\mathbf{r})$. This points out that the electron density to be used is not the unperturbed equivalent-crystal electron density, but it must include screening effects as well. In particular, second neighbors have a cage of nearest neighbors screening their movements (see, e.g., Fig. 1 of Ref. 21). Thus for second neighbors,

$$E_1+E_2 \propto R^p e^{-\alpha R} e^{-R/\lambda}\ , \tag{25}$$

where the stronger screening of second neighbors is included via the screening function $e^{-R/\lambda}$.

Actually, $F^*[a_1^*(i)]$ is to represent a distance-dependent component of the perturbation to *all* orders. For finite-sized perturbations, one must take into account not only electrostatic energies, but changes in kinetic, exchange, and correlation energies due to the perturbation. In other words, we have nonlinear or higher-order effects involved, which are not generally well represented by the two lowest-order perturbation terms on the ground-state single crystal. Going to higher order would severely complicate the calculation, however. Thus we attempt to make the perturbation as small as possible. We accomplish this by carrying out the perturbation not on the ground-state crystal, but rather on an equivalent crystal. We, in fact, can adjust the lattice constant of the equivalent crystal until the perturbation integral is zero. Combining Eqs. (3), (24), and (25), we have for metals and semiconductors

TABLE I. Computed constants. The constant p is $2n-2$, where n is the atomic principal quantum number, l (in Å) is computed from Eq. (10), λ (in Å) from Eq. (45), A_3 from Eqs. (48), (50), or (54), A_4 from Eqs. (49), (51), or (55), and D from Eq. (35). Note there is no constant A_1 defined, and A_2 can be found in Eqs. (34), (37), and (38). D, aA_2, and A_3 are dimensionless, where a is the crystal lattice constant. For metals, α (in Å^{-1}) is computed by requiring agreement with the experimental vacancy formation energy (Table II). For Si, Ge, and diamond, α is determined from the requirement that the computed vacancy formation energy of a frozen lattice (without relaxation of the vacancy neighbors) be equal to the cohesive energy, i.e., by assumption of bond additivity (Refs. 24 and 25).

Element	p	l	α	λ	$10^{-2}A_3/D$	$10^{-1}A_4/D$	$10^{-4}D$
Al	4	0.336	2.105	0.944	7.822	2.104	591.4
Cu	6	0.272	2.935	0.765	5.784	2.530	99.74
Ag	8	0.269	3.337	0.756	5.390	2.285	12.90
Au	10	0.236	4.339	0.663	4.047	1.673	1.127
Ni	6	0.270	3.015	0.759	7.382	2.793	100.1
Pd	8	0.237	3.612	0.666	5.242	2.012	11.25
Pt	10	0.237	4.535	0.666	5.789	1.727	1.071
Fe	6	0.277	3.124	0.770	9.183	1.887	60.62
W	10	0.274	4.232	0.770	12.03	1.497	1.179
C	2	0.253	2.017	0.711	24.50	1.511	1979.0
Si	4	0.344	2.177	0.967	16.96	1.059	267.8
Ge	6	0.348	2.857	0.978	17.22	1.360	36.48

$$N_1 R_{ec}^{p} e^{-\alpha R_{ec}} + N_2 (c_2 R_{ec})^{p} e^{-(\alpha+1/\lambda)c_2 R_{ec}} - \sum_{\text{defect NN}} R_j^{p} e^{-\alpha R_j} - \sum_{\text{defect NNN}} R_j^{p} e^{-(\alpha+1/\lambda)R_j} = 0 , \tag{26}$$

where

$$R_j \equiv |\mathbf{R}_j - \mathbf{R}_i| , \tag{27}$$

N_1 and N_2 are the number of equivalent-crystal nearest and next-nearest neighbors, respectively, R_{ec} is the equivalent-crystal nearest-neighbor distance we are solving for, c_2 is the ratio between the next-nearest-neighbor distance and the nearest-neighbor distance in the undistorted crystal, λ is the electronic screening length [see Eq. (45)],

$$p \equiv 2n-2 , \tag{28}$$

and n is the atom principal quantum number. The sums are over the actual defect crystal, the first over nearest neighbors and the second over next-nearest neighbors to atom i. Values of l, λ, p, and α and, indeed, all the other parameters in the following equations can be found in Table I. They are computed from the input data listed in Table II for a series of metals and covalent solids. One solves Eq. (26) for R_{ec}, obtains $a_1^*(i)$ from Eq. (22), and then obtains $F^*[a_1^*(i)]$ via Eq. (21).

For anisotropic deformations, there are an infinity of neighbor distance distributions for each average neighbor distance. In general, each of these distance distributions could be expected to have a different total energy even if they all have the same average distance. Further, bond angles can be altered via anisotropic deformations. Bond-angle effects involve three- and higher-atom clusters, as will be seen below.

Let us first consider a two-atom anisotropic effect. Suppose, e.g., that some neighbors are missing so that the

TABLE II. Experimental input. Cohesive energies (in eV) are from Ref. 32, elastic constants (in 10^{12} dyn/cm^2) are from Ref. 33, and metal vacancy formation energies (in eV) are from Ref. 22.

Element	Cohesive energy	Lattice constant	Vacancy formation energy	C_{11}	C_{12}	C_{44}
Al	3.34	4.04	0.66	1.143	0.619	0.316
Cu	3.50	3.61	1.30	1.762	1.249	0.818
Ag	2.96	4.08	1.19	1.314	0.973	0.511
Au	3.78	4.07	0.96	2.016	1.697	0.454
Ni	4.44	3.51	1.60	2.612	1.508	1.317
Pd	3.94	3.89	1.4	2.341	1.761	0.712
Pt	5.85	3.92	1.3	3.580	2.536	0.774
Fe	4.29	2.86	1.60	2.360	1.340	1.190
W	8.66	3.16	4.00	5.326	2.050	1.631
C	7.37	3.57		10.79	1.24	5.78
Si	4.64	5.43		1.677	0.6498	0.8036
Ge	3.87	5.66		1.3111	0.4923	0.6817

average neighbor distance is larger than R_0. The average neighbor distance can be lowered by decreasing the neighbor distances of the remaining atoms. This may cause some of the neighbor distances to become less than R_0, even while the average distance is greater than R_0. Compressing bonds below R_0 should contribute to an increase in the energy, which would oppose a decrease due to $F^*[a_1^*(i)]$. Thus clearly there is a two-atom anisotropic term, $F^*[a_2^*(i,j)]$, which is nonzero when nearest-neighbor bond lengths are anisotropic, i.e., when $R_j \neq R_0$, where R_0 is the bulk nearest-neighbor distance. Here we take the origin at atom i, so that the bond length to atom j is $R_j \equiv |\mathbf{R}_j|$. This is depicted in Fig. 4(c) for the diamond structure. As discussed above, one can treat semiconductor bonds as independent[24,25] for purposes of computing bond-length anisotropy energies. This means that one can obtain an anisotropy term $F^*[a_2(i,j)]$ for each neighbor j. The $E_p(a_2^*(i,j))=0$ equation for semiconductors is

$$N_1 R_{ec}^p e^{-\alpha R_{ec}} - N_1 R_0^p e^{-\alpha R_0} + A_2 R_0^p (R_j - R_0) e^{-\alpha(R_j - R_0)} = 0 , \quad (29)$$

where in this case R_{ec} is the nearest-neighbor distance for the equivalent crystal associated with the deviation of nearest-neighbor bond length R_j from R_0, and R_0 is the bulk nearest-neighbor distance at whatever pressure the solid is maintained at (see Fig. 4). Generally R_0 can be taken to be the ground-state, zero-pressure value since most experiments are done at atmospheric pressure. While $F^*[a_1^*(i)]$ is a many-atom term for metals and semiconductors which depends on average neighbor distances, for semiconductors $F^*[a_2^*(i,j)]$ is a two-atom term. The procedure for obtaining the associated energy is analogous to that for Eq. (26), namely one solves Eq. (29) for R_{ec}, obtains $a_2^*(i,j)$ from Eq. (22), and then finds $F^*[a_2^*(i,j)]$ from Eq. (21). Finally, $F^*[a_2^*(i)]$ is obtained from Eq. (28). Note that $R_{ec}=R_0$ if the deformation is isotropic, so that in that case $a_2^*(i,j)=0$ and $F^*[a_2^*(i,j)]=0$. Thus Eq. (29) is a bond-length anisotropy term, as discussed above.

For metals, it is well known that multiple-atom terms would be more important than they are for semiconductors. Bond-angle anisotropies will be included via three- and four-atom terms subsequently [Eqs. (39) and (40)]. Multiple-atom terms in bond-length anisotropies should also be expected to be important for metals, however. Including several of these higher-order bond-length terms for metals could complicate the method. There is a simpler approach, however. Equation (29) can be transformed into a many-atom term for metals by summing over all nearest neighbors:

$$N_1 R_{ec}^p e^{-\alpha R_{ec}} - N_1 R_0^p e^{-\alpha R_0} + A_2 R_0^p \sum_j (R_j - R_0) e^{-\beta(R_j - R_0)} = 0 , \quad (30)$$

where $\beta=4\alpha$ for the metals listed in Table II. For metals, one solves Eq. (30) for R_{ec}, obtains $a_2^*(i)$ from Eq. (22), and hence $F^*[a_2^*(i)]$ from Eq. (21). For metals, $F^*[a_2^*(i)]$ is a many-atom term which replaces $\sum_j F^*[a_2^*(i,j)]$ in Eq. (20). In this way semiconductor bond lengths are treated as independent in Eq. (29), while for metals multiple-atom effects are explicitly included in Eq. (30), consistent with the known fundamental nature of the two classes of materials.

As shown in the Appendix, the force corresponding to the bond-length anisotropy term is zero when $R_j=R_0$, as one would expect. Because of the exponentials, the perturbation of Eqs. (29) and (30) tends to die away rapidly for $R>R_0$, and rise rapidly for $R<R_0$. This is consistent with the well-known physical property that it is difficult to compress bonds below the bulk nearest-neighbor distance, while bond-length anisotropies become less important at larger bond lengths because interactions decay exponentially with distance. These behaviors tend to be exponential because of wave-function overlap.

The constant A_2 in those equations has yet to be determined. Its computation is also helpful in understanding the form of the equations. Let us start with an unperturbed semiconductor crystal. Next change the bond length to one of the nearest neighbors to atom i by $R-R_0$. We look now for an approximate expression for the energy increase $\delta\varepsilon_1$ due to this anisotropic deformation. For an isotropic change by the same distance, the energy increase would be

$$\varepsilon_i = \Delta E\, F^*[a^*] , \quad (31)$$

where

$$a^* = (R - R_0)/lc , \quad (32)$$

according to Eq. (22). Let us assume that the energy increase due to the change of a *single* bond length by $R-R_0$ is the energy increase *per bond* of the isotropic distortion:

$$\delta\varepsilon_i = (\Delta E/N_1) F^*[a^*] , \quad (33)$$

where again a^* is given by Eq. (32). We are now ready to find A_2. A_2 is determined such that $(\partial^2 \delta\varepsilon_i/\partial R^2)_0$ from Eqs. (32) and (33) agrees with that obtained from Eqs. (28) and (29). The result for cubic semiconductors is

$$a A_2/D = 2/\sqrt{3} , \quad (34)$$

where D is given by

$$D = N_1 e^{-\alpha R_0}(\alpha R_0 - p) , \quad (35)$$

and a is the lattice constant.

For metals, where bonds cannot be treated independently, we vary all neighbor bond lengths to atom i by $R-R_0$. Then

$$\delta\varepsilon_i = \Delta E\, F^*[a^*] , \quad (36)$$

where a^* is again given by Eq. (32). A_2 is again determined by requiring that $(\partial^2 \delta\varepsilon_i/\partial R^2)_0$ from Eqs. (32) and (36) agrees with that obtained from Eqs. (30) and (14). The result is

$$a A_2/D = 1/6\sqrt{2} \quad (37)$$

for fcc metals, and

$$aA_2/D = 1/4\sqrt{3} \tag{38}$$

for bcc metals.

Several comments are in order here. First, in combining Eqs. (36) and (30), we are in essence requiring an anisotropic expression [Eq. (30)] to agree with the result of an isotropic deformation. This is important because we would not want anisotropic energetics to be inconsistent with isotropic energetics. Remember also that the anisotropic expressions in Eqs. (29) and (30) are zero for isotropic deformations [see discussion below Eq. (29)]. Second, we deal with the second derivation rather than the first, because the latter is zero at equilibrium. Finally, the form of Eqs. (29) and (30) is designed so that energy second derivatives can be equal at equilibrium as in the above analysis.

Of course we might not only have anisotropic bond lengths, but also bond angles might deviate from that of the undistorted single crystal. The first bond-angle effect involves three atoms, which is accounted for by the third term $F^*[a_3^*(i,j,k)]$. This term is nonzero when the angle θ_{jk} included between R_j and R_k deviates from the undistorted single-crystal value. This is depicted for the diamond structure in Fig. 4(d). The $E_p(a_3^*(i,j,k))=0$ equation is for both metals and semiconductors:

$$N_1 R_{\rm ec}^p e^{-\alpha R_{\rm ec}} - N_1 R_0^p e^{-\alpha R_0} + A_3 R_0^p e^{-\alpha(R_j+R_k-2R_0)} \sin|\theta_{jk}-\theta| = 0 , \tag{39}$$

where $R_{\rm ec}$ is for the equivalent crystal associated with anisotropic distortion due to a difference between the nearest-neighbor bond angle θ_{ij} and the ground-state crystal bond angle θ and A_3 can be written in terms of the elastic constants as shown in Sec. II E 6. Here θ_{jk} is the bond angle included between bond lengths R_j and R_k and $\theta=70.5°$ for bcc, $\theta=90°$ for fcc, and $\theta=109.5°$ for the diamond structure—see Fig. 5. Clearly if $\theta_{jk}=\theta$, $R_{\rm ec}=R_0$ and $F^*[a_3^*(i,j,k)]=0$, so Eq. (39) contributes only when there is bond-angle anisotropy, as discussed above. We know that angular effects should become relatively less important as bond lengths become large. This is the reason there is an exponential function of bond lengths multiplying $\sin|\theta_{jk}-\theta|$. In complete analogy with the solutions of Eqs. (26), (29), and (30), one solves Eq. (39) for $R_{\rm ec}$, obtains $a_3^*(i,j,k)$ from Eq. (22), and then $F^*[a_3^*(i,j,k)]$ from Eq. (21). It is shown in the Appendix that the associated force is zero when $\theta_{jk}=\theta$, as expected intuitively. The magnitude of the angle is used as a matter of convenience so that $a_3^*(i,j,k)\le 0$. The bond angles are described in Figs. 4 and 5. For the applications of Sec. III, we found it made little difference whether $\sin|\theta_{jk}-\theta|$ or just $|\theta_{jk}-\theta|$ were used, because bond-angle distortions were relatively small.

The first three terms on the right-hand side of Eq. (20) are in principle sufficient for a simple description of solid surface or defect energetics when bonds can be considered as nearly independent, as in semiconductors.[24,25] For metals, however, electrons are relatively mobile and therefore bonds cannot be considered to be independent. We will see that in that case $F^*[a_2^*(i)]$ does not contribute to the shear elastic constants c_{44} and $c_{11}-c_{12}$ for cubic metals because $a_2^*(i)$ depends only on average neighbor distances. Because $F^*[a_1^*(i)]$ also only depends on average neighbor distances, it also does not contribute to either shear elastic constant in both cubic semiconductors and metals. Further, if ϵ is the strain associated with c_{44} shear, it turns out that $(\partial\theta/\partial\epsilon)_0=0$ for fcc metals. Thus $F^*[a_3^*(i,j,k)]$ does not contribute to c_{44} for the fcc structure, and so none of first three terms do.

This suggests that a four-atom term can make an important contribution to ε_i. This fourth and final perturbation term we call $F^*[a_4^*(i,p,q)]$. It depends on the difference of the face diagonals, d_p-d_q (see Fig. 5). For example, the fcc face diagonals are not equal in c_{44} shear, $d_p\neq d_q$, so c_{44} depends solely on $F^*[a_4^*(i,p,q)]$. The $E_p(a_4^*(i,p,q))=0$ equation for both metals and semiconductors is

$$N_1 r_{\rm ec}^p e^{-\alpha R_{\rm ec}} - N_1 R_0^p e^{-\alpha R_0} + A_4 R_0^p e^{-\alpha(R_j+R_k+R_l+R_m-4R_0)} |d_p-d_q|/d = 0 , \tag{40}$$

where the four distances in the exponential multiplying $|d_p-d_q|$ are the nearest-neighbor distances to atoms at the ends of the face diagonals, $R_{\rm ec}$ is for the equivalent crystal associated with anisotropic distortion due to a difference in lengths of face diagonals, $d_p-d_q\neq 0$, d is the face diagonal of the undistorted cube, and A_4 can be written in terms of the shear elastic constants as shown in Sec. II E 6. Because this anisotropy term should become small as bond lengths become large, we have the exponential function of bond lengths multiplying the $|d_p-d_q|$. Equation (40) leads to an $R_{\rm ec}\neq R_0$ when $d_p\neq d_q$, and thus $F^*[a_4^*(i,p,q)]\neq 0$. As with the other energy terms, the associated force is zero when $d_p=d_q$, as expected. This is shown in the Appendix. Note that the face diagonal distances do not depend directly on the coordinates of atom i, even though this four-atom energy is attributed to atom i. The only requirement is that the atoms at the corners of the faces be nearest neighbors to atom i. The thinking behind attributing this energy to atom i is based on a local energy density picture and the fact that atom i is located roughly at the center of the volume enclosed by the cube faces.

Since $d_p=d_q$ in $c_{11}-c_{12}$ shear for all cubic metals and semiconductors, $F^*[a_4^*(i,p,q)]$ does not contribute to $c_{11}-c_{12}$ for any of those solids. Further, $F^*[a_2]$ also does not contribute to $c_{11}-c_{12}$ for any of those solids. Thus $c_{11}-c_{12}$ depends only on $F^*[a_3(i,j,k)]$ for all cubic metals and semiconductors.

Next let us consider some of the geometrical aspects of computing bond-length, bond-angle, and face diagonal

anisotropy energies. Consider an atom in the fcc structure. There are three (100) planes intersecting this atom in the bulk single crystal. There are four nearest-neighbor atoms in each of these three planes. Each (100) plane contains four bond angles θ included between four corresponding pairs of nearest-neighbor position vectors and one pair of diagonal distances d_p and d_q. Thus there are twelve bond angles, twelve bond lengths, and three diagonal distance pairs all together. Consider now an atom in the bcc structure. There are twelve bond angles and eight bond lengths all together, involving the atom's eight nearest neighbors. There are six diagonal distance pairs associated with the six faces of the cube which has the eight nearest neighbors at its corners. For an atom in the diamond structure, there are six bond angles, four bond lengths, and three pairs of diagonal distances all together, involving the atom's four nearest neighbors. There is one bond angle and one diagonal distance for each cube face.

Because the total energy is written as an analytic expression, one can straightforwardly evaluate its gradient and determine the total force on each atom in the surface or bulk defect. The Appendix contains an analytic expression for the force, which can be useful for molecular-dynamics calculations or for locating energy minima in static calculations.

2. Simplest case

Consider a rigid defect such as a vacancy or a rigid solid surface where atoms are not allowed to relax around the surface or defect. In that case, bond lengths are either equal to R_0 or are infinite (the latter corresponding to atoms that are removed). Thus Eqs. (21), (22), (29), and (30) yield $F^*[a_2^*(i)]=0$. Similarly, all bond angles $\theta_{jk}=\theta$, so Eqs. (21), (22), and (39) yield $F^*[a_3^*(i,j,k)]=0$. Also $d_p=d_q$ so Eqs. (21), (22), and (40) yield $F^*[a_4^*(i,p,q)]=0$. Thus only $F^*[a_1^*(i)]\neq 0$ in this case. The solution of Eq. (26) is particularly simple, since all nearest-neighbor distances $=R_0$ and all next-nearest-neighbor distances $=c_2R_0$. Typically, one can obtain such energies with a hand calculator.

An example would be the surface energies computed for the "rigid" configuration listed in Table III or "ideal" configuration of Table X. In this case rigid and ideal mean the same thing, i.e., unrelaxed. One can see that there is excellent agreement with first-principles calculations, despite the simplicity of the equivalent-crystal-theory calculation. One can also see from Table III that the relaxation energies at metal surfaces are quite small. The results listed in Tables III and X will be more fully discussed in Sec. III.

3. Whistles and bells

For some problems, neighbor distances may not fall in neat nearest-neighbor and next-nearest-neighbor categories. This introduces a problem in defining next-nearest neighbors for screening purposes. Two examples are surface reconstruction, as we will consider in Sec. III for Si(100), and slip.[20] This is not a problem for the computation of $a_2^*(i,j)$ for semiconductors or $a_2^*(i)$ for metals, or for $a_3^*(i,j,k)$ and $a_4^*(i,p,q)$ for metals and semiconductors, because the exponential prefactors provide a gradual damping as R_j increases [see Eqs. (29), (30), (39), and (40)]. It is a consideration for the computation of $a_1(i)$, however, where second neighbors and beyond are screened more strongly than nearest neighbors [see Eq. (26)]. Thus we treat this ambiguity via an interpolation formula $S(R)$ for the screening length $1/\lambda$ for both metals and semiconductors:

$$N_1 R_{\rm ec}^p e^{-\alpha R_{\rm ec}} + N_2 (c_2 R_{\rm ec})^p e^{-(\alpha+1/\lambda)c_2 R_{\rm ec}} - \sum_{\rm defect} R_j^p e^{-[\alpha+S(R_j)]R_j} = 0 , \quad (41)$$

where the sum over the defect crystal or surface is over all neighbors, and for $R \le R_0$,

$$S(R)=0 , \quad (42)$$

for $R_0 \le R \le c_2 R_0$,

$$S(R)=(1/2\lambda)\{1-\cos[\pi(R-R_0)/(c_2R_0-R_0)]\} , \quad (43)$$

and for $R \ge c_2 R_0$,

$$S(R)=1/\lambda . \quad (44)$$

The differences between Eqs. (26) and (41) are unimportant for most calculations. Also, for most calculations the exponential multiplying the sin term in Eq. (39) and that multiplying $|d_p-d_q|$ in Eq. (40) can be taken to be equal to 1. For example, this is true for the surface relaxation calculations on metals to be presented in Sec. III because nearest- and next-nearest-neighbor distances are typically within 0.1 Å of the bulk, ground-state values.

4. How to use it

As mentioned earlier, the method has very modest numerical requirements, which is important for its intended application to low-symmetry-materials phenomena. The only equations that need to be solved are Eqs. (26), (39), (40), and either (29) or (30). Note that these equations are independent, and so one only has to solve one algebraic equation for one unknown at a time. There are, e.g., for the diamond structure a maximum of 14 independent algebraic equations in one unknown to solve [one from Eq. (26), four from Eq. (29), six from Eq. (39), and three from Eq. (40)]. The effort required for the solution truly is trivial. Once one knows the $R_{\rm ec}$ values from Eqs. (26), (29), (39), and (40), the total energy is obtained immediately via Eqs. (20)–(22). So the rate-limiting step of the method is the solution of the perturbation Eqs. (26), (39), and (40), and either (29) or (30). Equations (29), (30), (39), and (40) involve only nearest neighbors, while Eq. (26) is summed to second neighbors. It is shown in Sec. III (see, e.g., Table V), that second neighbors make quite small contributions because of screening. Thus the long-range sums that one often has to deal with in pair-potential approaches are not found here. One should remember that many-atom effects are contained in the universal energy relation, Eq. (12), but the relation does not involve long-range sums for its computation. Rather, it is represented by a simple analytic form. Each of the perturbation

equations is not coupled to the others, and involves only one unknown, R_{ec}. So the basic problem of the method is the solution of one equation at a time for one unknown. This is done only for those atoms in the solid whose neighbors are significantly perturbed from their equilibrium positions, because all other atoms have $\varepsilon_i=0$ [see Eqs. (20) and (21)].

Each equation to be solved is nonlinear. There are many methods available for solving nonlinear equations in one unknown. All of these methods are aided by the choice of good starting values. As we will see in Sec. III, the dominant defect or surface energy is often coming from the rigid defect or surface formation energy, for which the only nonzero term is $F^*[a_1(i)]$. This is the "simplest case" discussed in Sec. II E 2, and indeed can often be solved with a hand calculator. Thus it is a good starting point. For that starting point, the $R_{ec}=R_0$ for Eqs. (29), (30), (39), and (40). Also from that starting point it is straightforward to associate neighbors with particular positions in the cubic unit cell, as shown in Figs. 4 and 5. This allows the angles θ and diagonal distances d_p to be identified with crystalline starting values and followed as reconstruction or other distortions occur. From those starting values, one can then allow the atomic positions to relax or reconstruct to lower the total defect or surface formation energy ε.

It is typically easier to bend bond angles and alter face diagonals when neighbors are missing, although it is difficult to know quantitatively how much less energy is required. Thus in applying Eqs. (39) and (40), we adopted the convention that if an atom were missing one or more nearest neighbors, then we took $F^*[a_3^*(i,j,k)]=0$ and $F^*[a_4^*(i,p,q)]=0$ for that atom. Quantitatively this is a small effect for the applications of Sec. III.

There is a well-known problem of subsidiary minima found in many methods in the search for the absolute energy minimum. We did not encounter such a problem in all of the examples discussed in Sec. III. For example, in the (2×1) reconstruction of Si(100), we varied 14 independent atomic coordinates simultaneously, and found the same absolute minimum for a broad variety of starting points. Incidentally, this problem was easily solved on a personal computer.

5. *Electronic screening*

Some further comments about electronic screening are in order at this point. First, we know of no other method of this type in which electronic screening effects are taken into account. We will see in Sec. III that they are indeed important (see, e.g., Table V). Second, while the screening length λ appears explicitly in the second-neighbor terms of Eq. (26), there is screening even of nearest-neighbor movements. This is reflected in α being different from the atomic value.

The value of α appropriate for solids is derived empirically as follows. For metals, α is varied until the computed vacancy formation energy is equal to the experimental value[22] listed in Table II. It is clear from the review by Wollenberger[22] that experimental values of the vacancy formation energy for many metals have converged over the years to a scatter of the order of 0.1 eV or less. Further, calculations for bcc metals suggest that energies of relaxation around the vacancy appear to be also 0.1 eV or less.[23] Thus α is determined for metals so that the energy to form a rigid or unrelaxed vacancy is equal to the experimental value.

For metals, the electrons are very capable of strengthening remaining bonds when some are broken. For example, if there were no bond strengthening, the vacancy formation energy would be precisely equal to the cohesive energy. Table II shows that for metals the vacancy formation energy is roughly in the range of $\frac{1}{5}-\frac{1}{2}$ of the cohesive energy. For semiconductors (see, e.g., Ref. 24), and organic compounds,[24,25] bond additivity can be rather accurate if only one or perhaps two bonds per atom are broken. This is fortunate because relaxation around a vacancy in, say, Si or diamond, can be rather complex, involving Jahn-Teller distortions, a significant complication. Results of first-principles calculations[26] of vacancy-formation energies in Si cover the relatively broad range of 3.6–5.0 eV. Here we take advantage of bond additivity and assume that the energy to form a rigid or unrelaxed vacancy in Si, Ge, or diamond is equal to the respective cohesive energy. Since we then have a formation energy associated with known atomic positions, we can straightforwardly compute α for these materials in a manner consistent with the way we determined α for metals. The resultant α values are shown in Table I. We will see in Sec. III that this approach leads to accurate results for Si.

The computation of the screening length λ is not necessarily straightforward for anything but simple metals. For the latter, Pines[27] has found that $\lambda=1.58$ Å for Na. For transition metals or semiconductors the Bohm-Pines free-electron picture is oversimplified, however. For transition metals and semiconductors one can have directional electronic charge distributions which do not resemble an isotropic free-electron picture. However, some of us[10] have argued that energy curves ought to scale on to a universal form if the length scale were taken to be proportional to the electronic screening length. In fact, for transition metals[12] the cohesive energy curves can be scaled on to a universal form both via scaling lengths l [see Eq. (8)], as in Fig. 2, and via screening lengths. The screening lengths were computed via the Bohm-Pines expression, taking the free-electron density to be the computed interstitial electron density as suggested by Moruzzi, Janak, and Williams.[28] Such screening lengths are at best approximate for transition metals. Perhaps one can obtain more accurate screening lengths by noting that if both screening lengths λ and scaling lengths l can scale the energy relation into a universal form, then λ and l must be proportional. That is,

$$\lambda=\lambda_{Na}(l/l_{Na})=2.81l\ , \tag{45}$$

where we have taken the Bohm-Pines value for λ_{Na} and the computed value for l_{Na}. Screening lengths λ from Eq. (45) are tabulated for simple and transition metals as well as semiconductors in Table I.

As stated above and shown in Eq. (26), atoms that are at second-neighbor distances and further have their per-

turbation terms multiplied by the screening factor $e^{(-1/\lambda)R}$. This takes into account the enhanced screening due to a full cage of nearest neighbors, which has been seen in first-principles calculations (see Fig. 1, Ref. 21). One could rightly argue that since the nearest-neighbor movements are screened, the second-neighbor screening enhancement factor would be too strong if it involved the full screening length λ. However, since α is determined empirically via Eq. (26) to give the experimental vacancy formation energy, then presumably the resultant α will be appropriately adjusted. The important point is that relative screening lengths of the different solids are correctly represented by a combination of Eqs. (26) and (45).

Finally, while Eq. (26) has general applicability, one can envision the possibility of enhanced screening for some nearest neighbors as well. This is an exception which generally one would not have to be concerned with, but one must be aware of the possibility. Consider a metal surface. There the screening tends to be planar and surface effects screen rapidly with depth into the metal, with surface screening lengths[29] of the order of 0.5 Å. If a crystal were cleaved to produce a high-index plane, it is possible for a plane of atoms deeper than the surface plane to be missing nearest neighbors. In this case even nearest-neighbor removal could be screened out and should be treated in Eq. (26) with the enhanced screening factor $e^{(-1/\lambda)R}$. The only example of this that we found in Sec. III was for the fcc (110) surface. There the second layer is missing a nearest neighbor, and so for that layer the term $N_1 R_{ec}^{p} e^{-\alpha R_{ec}}$ in Eq. (26) should be replaced by

$$(N_1-1)R_{ec}^{p}e^{-\alpha R_{ec}}+R_{ec}^{p}e^{-(\alpha+1/\lambda)R_{ec}} .$$

This is a small change [8% decrease of the surface energy of Cu(110)], but is technically more correct. For the lower-index metal surfaces and the semiconductor (100) or (111) surfaces, the second layer is not missing any nearest neighbors, and so Eq. (26) applies as written. Equation (26) is unaltered in application to point defects as well, because there the screening charge decays essentially radially, completely consistent with the form of the equation.

6. *Analytic determination of A_3 and A_4*

It remains to specify the constants A_3 and A_4. This will now be done. While equivalent-crystal theory is an atomistic method which, as we will see later, can be applied to short-range, local defects, continuum elasticity theory typically is limited to longer-range, more slowly varying defects. It is valuable to make a quantitative connection between the two theories, so that equivalent-crystal results might be consistent with continuum results in the appropriate limits. It is with this in mind that we determine A_3 and A_4 so that there is exact agreement with the experimental elastic constants c_{44} and $c_{11}-c_{12}$.

As noted above Eq. (26), $F^*[a_1^*(i)]$ makes no contribution to the shear elastic constants c_{44} and $c_{11}-c_{12}$ of both cubic metals and semiconductors, because the average bond length does not change to first order in these deformations. For the same reason, Eq. (30) does not contribute to these elastic constants for metals.

Thus for metals, from Eqs. (20) and (21),

$$c_{44}=(\Delta E/\Omega_0)\left[\sum_{j,k}[\partial a_3^*(i,j,k)/\partial e_{xy}]_0^2 + \sum_{p,q}[\partial a_4^*(i,p,q)/\partial e_{xy}]_0^2\right], \quad (46)$$

where the subscript 0 refers to the ground-state crystal, Ω_0 is the volume per atom, and e_{xy} is the strain associated with c_{44}. Similarly, for metals

$$c_{11}-c_{12}=(\Delta E/2\Omega_0)\left[\sum_{j,k}[\partial a_3^*(i,j,k)/\partial \xi]_0^2 + \sum_{p,q}[\partial a_4^*(i,p,q)/\partial \xi]_0^2\right], \quad (47)$$

where ξ is the strain associated with $c_{11}-c_{12}$. Combining Eqs. (22), (39), (40), (46), and (47), we find for fcc metals,

$$A_3/D=(1/6\sqrt{3})\sqrt{(c_{11}-c_{12})/B} \quad (48)$$

and

$$A_4/D=\tfrac{1}{3}\sqrt{c_{44}/B} . \quad (49)$$

Note that in the case of fcc metals, c_{44} is determined entirely by the bond-angle term and $c_{11}-c_{12}$ depends only on the face diagonal term.

For bcc metals,

$$A_3/D=(1/2\sqrt{2})\sqrt{(c_{11}-c_{12})/9B} \quad (50)$$

and

$$A_4/D=(1/3\sqrt{2})\sqrt{c_{44}/B-(c_{11}-c_{12})/9B} . \quad (51)$$

For semiconductors, the bond-length anisotropy term can be computed as if the bonds were independent, as discussed earlier.[25] Thus that term can contribute to both shear elastic constants in semiconductors:

$$c_{44}=(\Delta E/\Omega_0)\left[\sum_{j}[\partial a_2^*(i,j)/\partial e_{xy}]_0^2 + \sum_{j,k}[\partial a_3^*(i,j,k)/\partial e_{xy}]_0^2 + \sum_{p,q}[\partial a_4^*(i,p,q)/\partial e_{xy}]_0^2\right] . \quad (52)$$

Similarly,

$$c_{11}-c_{12}=(\Delta E/2\Omega_0)\left[\sum_{j}[\partial a_2^*(i,j)/\partial \xi]_0^2 + \sum_{j,k}[\partial a_3^*(i,j,k)/\partial \xi]_0^2 + \sum_{p,q}[\partial a_4^*(i,p,q)/\partial \xi]_0^2\right] . \quad (53)$$

The diamond structure is a bit more challenging, because of the possibility of internal strain.[30,31] In the case of c_{44} shear, the energy can be lowered by relieving length anisotropy at the expense of bond-angle anisotropy. This is done by one fcc sublattice displacing relative to the other in the z direction by $\zeta e_{xy} a/4$, where a is the lattice constant. The internal displacement parameter ζ is varied until the c_{44} strain energy is a minimum. The results are

$$A_3/D=\tfrac{1}{2}\sqrt{(c_{11}-c_{12})/9B}\ , \tag{54}$$

$$A_4/D=\tfrac{1}{3}[c_{44}/B-4(\tfrac{1}{2}+\zeta)^2(c_{11}-c_{12})/9B -(1-\zeta)^2]^{1/2}\ , \tag{55}$$

and

$$\zeta=(t^2-u^2)/(t^2+2u^2)\ , \tag{56}$$

where $t^2\equiv(aA_2/D)^2/2$ and $u^2\equiv\frac{16}{3}(A_3/D)^2$.

Resultant values of A_3 and A_4 are listed in Table I for the bcc, fcc, and diamond lattices. We will see in Sec. III (Table VIII), that our computed values of ζ are in good agreement with experiment.

F. Working equation summary

It is important when a method is being introduced to derive the working equations and to discuss the physics behind the method, as we have attempted to provide in the preceding sections. This can tend to obscure the actual working equations and perhaps make the method appear to be more cumbersome than it really is. Thus in this section we gather together the equations one needs to solve for a typical problem. Most of these equations are written as they appeared in the preceding text, and hopefully it will be helpful to have them all together.

The example that we choose is cubic semiconductors such as Si, Ge, or diamond. One should preferably call diamond an insulator. We consider the common case where neighbors fall neatly into nearest- and next-nearest-neighbor categories. For the more general case, see Sec. II E 3. Equations for fcc and bcc metals are very similar to the following, and can be found in Sec. II E.

The defect or surface formation energy ε_1 is given by Eq. (20):

$$\varepsilon_i=\Delta E\left[F^*[a_1^*(i)]+\sum_j F^*[a_2^*(i,j)] +\sum_{j,k} F^*[a_3^*(i,j,k)]+\sum_{p,q} F^*[a_4^*(i,p,q)]\right]\ , \tag{57}$$

where [Eqs. (21) and (22)]

$$F^*[a^*]=1-(1+a^*)e^{-a^*} \tag{58}$$

and

$$a^*=(R_{ec}/c-r_{WSE})/l\ . \tag{59}$$

a_1^* is determined by Eq. (26):

$$N_1R_{ec}^p e^{-\alpha R_{ec}}+N_2(c_2R_{ec})^p e^{-(\alpha+1/\lambda)c_2R_{ec}} -\sum_{\text{defect NN}} R_j^p e^{-\alpha R_j}-\sum_{\text{defect NNN}} R_j^p e^{-(\alpha+1/\lambda)R_j}=0\ , \tag{60}$$

in combination with Eq. (59), where l, p, λ, and α can be found in Table I [see also Eqs. (28) and (45)]. Similarly, a_2^* is determined by Eq. (29):

$$N_1R_{ec}^p e^{-\alpha R_{ec}}-N_1R_0^p e^{-\alpha R_0} +A_2R_0^p(R_j-R_0)e^{-\alpha(R_j-R_0)}=0\ , \tag{61}$$

where A_2 can be read from Table I or computed from Eq. (34):

$$aA_2/D=2/\sqrt{3}\ , \tag{62}$$

where D is given by Eq. (35):

$$D=N_1e^{-\alpha R_0}(\alpha R_0-p)\ , \tag{63}$$

and a is the lattice constant.

a_3^* can be computed from Eq. (39):

$$N_1R_{ec}^p e^{-\alpha R_{ec}}-N_1R_0^p e^{-\alpha R_0} +A_3R_0^p e^{-\alpha(R_j+R_k-2R_0)}\sin|\theta_{jk}-\theta|=0\ , \tag{64}$$

and a_4^* from Eq. (40):

$$N_1R_{ec}^p e^{-\alpha R_{ec}}-N_1R_0^p e^{-\alpha R_0}+A_4R_0^p e^{-\alpha(R_j+R_k+R_l+R_m-4R_0)}|d_p-d_q|/d=0\ , \tag{65}$$

where A_3 and A_4 can be found in Table I or computed from Eqs. (54)–(56):

$$A_3/D=\tfrac{1}{2}\sqrt{(c_{11}-c_{12})/9B}\ , \tag{66}$$

$$A_4/D=\tfrac{1}{3}\sqrt{c_{44}/B-4.24(c_{11}-c_{12})/9B-0.221}\ . \tag{67}$$

In Eq. (67) we have inserted the value for the internal displacement parameter $\zeta=0.53$ (Table VIII) for Si.

It should be remembered that the working equations (60), (61), (64), and (65) are decoupled. Thus one is solving one equation at a time in one unknown, as noted in Sec. II E 4.

III. RESULTS

In this section we predict a number of defect or surface properties for metals and semiconductors. A comparison of the predictions with the results of first-principles cal-

culations and with experimental results provides a significant test of the method. We will see that generally there is excellent agreement with both experimental and first-principles results.

The experimental input to the method includes the three bulk elastic constants, the bulk cohesive energy, the bulk lattice constant, and the vacancy formation energy (see Table II). No fitting is required to determine the computed constants (Table I), because each of these quantities can be predicted analytically by the method, as shown in the preceding section.

Notice that there is no surface information in the input. This makes the accuracy of predicted surface properties a good test of the method. There is another reason why surface defect predictions are a particularly interesting test of the method. The method is based on perturbation theory, where the unperturbed system is a single crystal. Cleaving a solid to form a surface is a very strong perturbation indeed. Thus surface calculations provide a particularly difficult test for the method.

As the same formulation is used for both semiconductors and metals, it is of interest to carry out computations for both classes of solids and compare the accuracy. We begin with calculations for metal surfaces.

A. Metals

Recently, surface-energy values computed via first-principles techniques have begun to appear in the literature and so we will compare our predictions with them. The surface energy σ follows immediately from Eq. (20):

$$\sigma=\sigma_1+\sigma_2+\sigma_3+\sigma_4 , \tag{68}$$

where

$$\sigma_1=(\Delta E/A)\sum_i F^*[a_1^*(i)] , \tag{69}$$

$$\sigma_2=(\Delta E/A)\sum_i F^*[a_2(i)] , \tag{70}$$

$$\sigma_3=(\Delta E/A)\sum_{i,j,k} F^*[a_3(i,j,k)] , \tag{71}$$

$$\sigma_4=(\Delta E/A)\sum_{i,p,q} F^*[a_4(i,p,q)] , \tag{72}$$

and A is the surface area. The sum over i includes only one atom per atomic layer for a (1×1) surface structure, and usually only two to three layers need be included for metal low-index planes and five to six layers for semiconductors. This makes for a relatively trivial surface-energy computation.

Results for surface energies of selected fcc and bcc metals are shown in Table III. Our predictions are shown in the equivalent-crystal-theory (ECT) columns. Results are given for rigid or ideal surfaces and, for the fcc metals, (1×1) planar relaxed surfaces (see Fig. 6). First note that the relaxation energies are small, typically 5% or less of the surface energy σ. Second, the agreement with the first-principles calculations, done with the local-density approximation (LDA), is good. On average the ECT and LDA values are within 10%. Predictions from the embedded atom method[34] for the fcc metals and

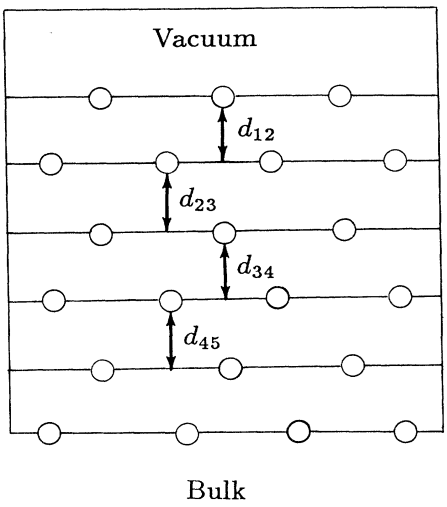

FIG. 6. Schematic showing interplanar spacings near the surface.

from the N-body potential method[3] for bcc metals are shown in the column labeled "other." These two semiempirical methods are about as simple to apply as ECT. The predictions of these other methods are 45–55% lower than the first-principles values. The reasons for these relatively large discrepancies are not clear.

It is interesting to compare the relative sizes of σ_1, σ_2, σ_3, and σ_4. These are shown in Table IV. The energy σ_1 derives from Eq. (26), the perturbation which depends only on average neighbor distances. One can see from Table IV that this term dominates σ. σ_2 derives from Eq. (30), i.e., from bond-length anisotropy, σ_3 derives from Eq. (39), i.e., from bond-angle anisotropy, and σ_4 derives from Eq. (40), i.e., from face diagonal anisotropy. While $\sigma_2>\sigma_3$ or σ_4, none is more than a few percent of σ_1. This is the first indication of how small these anisotropy terms can be for metals when there is not reconstruction. Later we will see that these terms can be relatively larger for reconstructed Si.

Next, we examine the effect of the enhanced second-neighbor screening. Table V shows rigid surface energies of Cu computed with λ values in Eq. (26) taken from Eq. (45) ("screened"), with $\lambda=\infty$ ("unscreened"), and in the nearest-neighbor approximation. One can see that the ordering according to crystal face of the unscreening surface energies is different from that of the screened energies. In particular, the unscreened Cu(100) surface energy is 27% lower than the screened value. Thus enhanced second-neighbor screening is certainly an important effect here. Comparison with the nearest-neighbor results shows that the latter are close to the screened results. This is evidence that the second-neighbor screening significantly weakens second-neighbor effects in defects and surfaces.

Now let us consider a somewhat more difficult problem, the (1×1) or planar relaxation of the fcc metal surfaces of Cu, Ni, Ag, and Al. These metals are known to relax in that fashion. In this calculation the movements

TABLE III. Surface energies, in erg/cm^2, are computed for some selected metals. Energies are computed in both a "rigid" configuration, in which the surface atoms are held in the same relative locations they would have had in the bulk, and a "relaxed" configuration, in which the atoms are allowed to relax to minimize the total energy. Equivalent-crystal-theory (ECT) predictions are compared with results of first-principles calculations within the local-density approximation (LDA). ECT predictions are rounded to the nearest 10 erg/cm^2.

Element	Crystal face	ECT rigid	ECT relaxed	LDA rigid	Other
Cu	(111)	1830	1780	2100[a]	1170[b]
	(100)	2380	2320	2300[c]	1280[b]
	(110)	2270	2210		1400[b]
Ag	(111)	1270	1230		620[b]
	(100)	1630	1600	1650[c]	705[b]
	(110)	1540	1510		770[b]
Ni	(111)	2400	2320		1450[b]
	(100)	3120	3040	3050[c]	1580[b]
	(110)	2980	2910		1730[b]
Al	(111)	920	860		
	(100)	1290	1220		
	(110)	1310	1230	1100[d]	
Fe	(110)	1820			
	(100)	3490		3100[c]	1693[e]
W	(110)	3330			
	(100)	5880		5200[f]	2926[e]

[a]Reference 35.
[b]Reference 34.
[c]Reference 36.
[d]Reference 37.
[e]Reference 3.
[f]Reference 38.

TABLE IV. Energy components of relaxed surface energies, in erg/cm^2, for some selected metals. The components are defined in Eqs. (68)–(72), and correspond to successive terms in Eq. (20) as well.

Element	Crystal face	σ_1	σ_2	σ_3	σ_4
Cu	(111)	1753.9	20.9	0.0	1.4
	(100)	2297.1	22.6	1.9	0.0
	(110)	2190.2	23.7	0.2	0.6
Ag	(111)	1219.5	12.4	0.0	0.7
	(100)	1581.1	13.4	1.0	0.0
	(110)	1496.2	12.2	0.1	0.2
Ni	(111)	2293.0	26.9	0.0	2.2
	(100)	3007.6	28.9	4.1	0.0
	(110)	2875.0	28.9	0.3	0.9
Al	(111)	841.2	20.6	0.0	1.0
	(100)	1186.8	26.1	3.9	0.0
	(110)	1201.3	28.3	0.3	0.5

TABLE V. Effect of second-neighbor screening on rigid surface energies of Cu. The results labeled "screened" are computed with λ values in Eq. (26) taken from Eq. (45) (as listed in Table I). Those labeled "unscreened" are computed with $1/\lambda=0$. For comparison, nearest-neighbor-only results are listed. Predictions are rounded to the nearest 10 erg/cm^2.

Crystal face	Screened	Unscreened	Nearest neighbor
(111)	1830	1790	1820
(100)	2380	1740	2380
(110)	2270	2100	2270

of the planes are coupled through the surface energy σ, and the equilibrium interplanar separations are those which minimize σ. See Fig. 6, where the interplanar spacings are defined schematically. Results are shown in Table VI. The changes of interplanar spacings are reported as a percentage of the bulk interplanar spacing. The absolute changes are quite small, being of order 0.1 Å or less. The relaxation energies are also small, in the range of 10–40 meV per surface atom. Thus this is a difficult test of the theory. Fortunately, accurate experimental results are available for these relaxation percentages. One can see from Table VI that the low-energy

TABLE VI. Percentage changes in interlayer spacing due to relaxation. The embedded-atom-method (EAM) results are from Ref. 34.

Element	$\Delta d_{n,n+1}$	ECT	EAM	Experiment	Technique (reference)
Cu(110)	Δd_{12}	−7.7%	−4.9%	(−8.5±0.6)%	LEED(39)
				(−7.5±1.5)%	Ion scattering(40)
	Δd_{23}	+3.4%	+0.2%	(+2.3±0.8)%	LEED(39)
				(+2.5±1.5)%	Ion scattering(40)
Cu(100)	Δd_{12}	−3.7%	−1.4%	(−2.1±1.7)%	LEED(41)
				(−1.1±0.4)%	LEED(42)
	Δd_{23}	+1.9%	−0.3%	(+0.45±1.7)%	LEED(41)
				(+1.7±0.6)%	LEED(42)
Cu(111)	Δd_{12}	−3.1%	−1.40%	(−0.7±0.5)%	LEED(43)
	Δd_{23}	+1.9%	−0.05%		
Ag(110)	Δd_{12}	−6.0%	−5.7%	−5.7%	LEED(42)
				(−7.8±2.5)%	Ion scattering(44)
	Δd_{23}	+2.8%	+0.3%	+2.2%	LEED(42)
				(+4.3±2.5)%	Ion scattering(44)
Ag(100)	Δd_{12}	−3.0%	−1.90%		
	Δd_{23}	+1.7%	−0.05%		
Ag(111)	Δd_{12}	−2.5%	−1.30%		
	Δd_{23}	+1.6%	−0.04%		
Ni(110)	Δd_{12}	−7.6%	−4.87%	(−8.7±0.5)%	LEED(45)
				(−9.0±1.0)%	Ion scattering(46)
	Δd_{23}	+3.4%	+0.57%	(+3.0±0.6)%	LEED(45)
				(+3.5±1.5)%	Ion scattering(46)
Ni(100)	Δd_{12}	−3.7%	−0.002%	(−3.2±0.5)%	Ion scattering(47)
	Δd_{23}	+2.0%	−0.001%		
Ni(111)	Δd_{12}	−3.1%	−0.05%	(−1.2±1.2)%	LEED(48)
	Δd_{23}	+1.9%	+0.00%		
Al(110)	Δd_{12}	−10.4%	−10.4%	(−8.6±0.8)%	LEED(49)
				(−8.5±1.0)%	LEED(50)
	Δd_{23}	+4.7%	+3.1%	(+5.0±1.1)%	LEED(49)
				(+5.5±1.1)%	LEED(50)
Al(100)	Δd_{12}	−4.9%			
	Δd_{23}	+1.8%			
Al(111)	Δd_{12}	−3.9%		(+0.9±0.7)%	LEED(51)
	Δd_{23}	+2.5%			

electron diffraction (LEED) and ion scattering results are in good agreement with each other. Next compare the ECT predictions with the experimental results. One can see that the theoretical predictions are typically within experimental error bars, often within 0.01 Å of experiment. This is surprisingly good accuracy. It would seem to be as good or better as one should expect from first-principles calculations, but the effort to perform the ECT calculation is relatively trivial. Also included in Table VI are embedded-atom-method (EAM) predictions. One can see that the EAM predictions are substantially smaller than experiment, particularly for Δd_{23} in every case and for both Δd_{12} and Δd_{23} for Ni. Reasons for such differences are not evident.

It is interesting to examine the relative contributions of σ_1, σ_2, σ_3, and σ_4 to final or equilibrium values of the interplanar spacing. Values of Δd_{12} are listed in Table VII for inclusion of all four terms, σ_1, σ_2, and σ_3 only ($A_4=0$), σ_1, σ_2, and σ_4 only ($A_3=0$), and σ_1, σ_3, and σ_4 only ($A_2=0$). Comparing the results using all terms with those having $A_4=0$ and $A_3=0$ shows that angular and face diagonal anisotropies play a very weak role in planar relaxations on these metals. This is consistent with the surface energy results of Table IV. The results listed in Table VII for $A_2=0$ tell quite a different story from the corresponding results of Table IV, however. While the bond-length anisotropy term makes only a small contribution to the surface energy, it is very important to the equilibrium interatomic distances. Surface relaxations are, after all, highly anisotropic. Since a surface atom is missing nearest neighbors, its $a_1^*(i)>0$. That is, the equivalent-crystal lattice constant of the lowest-order perturbation term lies to the right of the minimum of the universal energy relation, Fig. 2. Since $F^*[a_1^*(i)]$ depends only on average neighbor distances through Eq. (26), it is as if a surface atom were seeing a lowered neighbor density. To lower the energy via this first term, the system wants $a_1^*(i)$ to decrease toward 0, i.e., to move left toward the minimum in Fig. 2. This is accomplished by the surface layer moving toward the second layer, so that the neighbor density around the surface atoms is increased. In the process, however, some nearest-neighbor distances become $<R_0$, even while the *average* nearest-neighbor distance is $>R_0$. This is how the bond-length anisotropy is manifested. The reason $F^*[a_2^*(i,j,k)]$ contributes so little to the energy and yet so strongly to the spacing can be found in the form of Eq. (30). The form in that equation causes the bond-length anisotropy energy to rise rapidly with a decrease in R for $R<R_0$. Physically this is due to the large forces required to compress solid bonds below bulk nearest-neighbor distances. These large forces do not allow the interatomic distances to change very much (see Table VI), and so the associated energy change is very small. If one were to ignore these large forces, Table VII shows that the spacing changes would be much too large.

B. Semiconductors

In many ways, semiconductors with their more directional bonds and filled bands are quite different form metals. Despite that, we are attempting to have a single method which applies to both classes of materials. The presumptions are at least twofold. First, it is presumed that many properties of metals and semiconductors are similar. Second, it is hoped that differences will be manifested in different relative contributions of the four terms of Eq. (20).

One of the clear differences between, say, fcc or bcc metals and diamond structure semiconductors is found in

TABLE VII. Energy component effects on relaxation of interlayer spacings. The energy is relaxed by varying Δd_{12} and Δd_{23} simultaneously with $A_4=0$, $A_3=0$, and $A_2=0$, respectively, and with the other A values taken from Table I. Equilibrium results for Δd_{12} are listed. The Δd_{12} listed under "All" are computed with all of the energy components included, i.e., with all A_2, A_3, and A_4 values taken from Table I.

Element	Crystal face	All	$A_4=0$	$A_3=0$	$A_2=0$
Cu	(111)	−3.1%	−3.1%	−3.1%	−24.0%
	(100)	−3.7%	−3.7%	−4.0%	−22.0%
	(110)	−7.7%	−7.7%	−7.7%	−60.0%
Ag	(111)	−2.5%	−2.5%	−1.6%	−27.0%
	(100)	−3.0%	−3.0%	−3.0%	−19.0%
	(110)	−6.0%	−6.1%	−6.1%	−53.0%
Ni	(111)	−3.1%	−3.1%	−3.1%	−23.0%
	(100)	−3.7%	−3.7%	−4.0%	−17.0%
	(110)	−7.6%	−7.6%	−7.6%	−58.0%
Al	(111)	−3.9%	−4.0%	−3.9%	−39.0%
	(100)	−4.9%	−4.9%	−5.0%	−22.0%
	(110)	−10.4%	−10.4%	−10.6%	−89.0%

TABLE VIII. Internal displacement parameter ζ. Experimental values were taken from Refs. 52 and 53. The first-principles values (labeled LDA) were taken from Ref. 54.

Element	ECT	LDA	Experiment
C	0.27		
Si	0.53	0.53	0.74
Ge	0.52	0.44	0.72

c_{44} shear, as discussed below Eq. (53) in Sec. II. In that shear mode, diamond structure crystals can partly relieve the strain by displacement of one fcc sublattice relative to the other[30] in the z direction by $\zeta e_{xy} a/4$, where $e_{xy} a/4$ is the usual shear strain. As discussed in Sec. II, we computed the internal strain parameter ζ from the requirement that it minimize the shear strain energy. An analytic expression for ζ resulted, which is given in Eq. (56). We found $\zeta=0.27$ for diamond, $\zeta=0.53$ for Si, and $\zeta=0.52$ for Ge. The internal strain parameter ζ can be measured via x-ray diffraction[52,53] for two of the three nonmetallic materials treated here, Si and Ge. There is as yet no experimental value for diamond because, as explained in Ref. 52, reflection intensities are weak. The experimental results are compared with our predictions in Table VIII. One can see that the agreement is good. A first-principles calculation[54] has yielded $\zeta=0.53$ for Si and $\zeta=0.44$ for Ge, somewhat lower than the experimental values. That our predicted value for diamond is significantly smaller than those for Si and Ge is consistent with earlier predictions.[55] The semiempirical approach of Ref. 16 yielded $\zeta=0.74$ for Si and $\zeta=0.71$ for Ge, in good agreement with experiment.

Next let us consider the Si(100) surface. Although this surface is known to reconstruct, it is nevertheless of interest to first compute changes in interlayer spacings for (1×1) relaxations because there are first-principles results to compare with. Predicted percentage changes in interlayer spacings are presented in Table IX. For Si(100), the ECT value of Δd_{12} compares well with the first-principles result of Ref. 24. However, the latter authors show a small compression of d_{23} while we find a small expansion. Next we present results for surface energies of ideal (rigid) and (1×1) relaxed Si(100). Results of our predictions can be found in Table X. One can see there is close agreement between the ECT predictions and the first-principles values from Ref. 24. On the other hand, the predicted values from Ref. 16 are substantially too low. Also the ideal (1×1) relaxation energy is an order of magnitude larger than computed here or in Ref. 24.

TABLE IX. Calculated percentage changes in interlayer spacings for (1×1) relaxations of Si(100).

Surface	$\Delta d_{n,n+1}$	ECT	Ref. 24
Si(100)	Δd_{12}	−5.1%	−5.0%
	Δd_{23}	+0.2%	−2.0%

There have been many investigations of Si(100) reconstruction.[56,57] While a number of models have been proposed, recent scanning tunneling microscopy (STM) measurements[57] have made a definitive identification of the surface structure. The STM images revealed a dimer type of reconstruction. The authors concluded that at room temperature the time-averaged configuration for the dimers is symmetric, although the dimers may be dynamically buckling about this equilibrium configuration on a time scale which is short compared to the STM measurement time. The symmetric dimer configuration is consistent with the first-principles results of Pandey.[58] As shown in Figs. 7 and 8, the symmetric dimer reconstruction involves substantial atomic displacements as deep as five atomic layers from the surface. We will see that the corresponding surface energy change is also large.

Our ECT calculation of the Si(100) dimer reconstruction required that 14 atomic coordinates be varied independently to minimize the total energy. This nevertheless was a fairly modest calculation which was easily carried out on a personal computer. Consistent with recent experimental and theoretical results, we find the symmetric dimer to have a lower energy than the asymmetric dimer, at least for a (2×1) configuration. The total energy versus symmetric dimer atomic spacing is shown in Fig. 7. The surface energy of the ideal (rigid) surface is indicated by the triangle, while that of the relaxed (1×1) surface is given by the circle. The energy of the (2×1) reconstructed surface is denoted by the square. These energies are also listed in Table X in the column under ECT. Figure 7 shows graphically that most of the energy drop is due to the reconstruction as opposed to the (1×1) relaxation, consistent with the first-principles results.[24,58,59] The dimer spacing at the minimum is 2.31 Å, slightly smaller than the bulk nearest-neighbor distance of 2.35 Å. At each spacing, the total energy is minimized by relaxing atomic positions in the top five atomic layers. One can see that the energy curve basically con-

TABLE X. Si(100) surface energies in erg/cm^2. The values in parentheses are in eV per surface atom. The (2×1) values are for symmetric dimer formation. For Refs. 58 and 59, they are computed by subtracting the relaxation energies reported in those references from the ideal surface energy of Ref. 24 (shown below). The ideal surface energy means the same thing as the rigid surface energy of Table I, i.e., unrelaxed.

Surface	ECT	Ref. 24	Ref. 58	Ref. 59	Ref. 16
Ideal	2850(2.63)	2740(2.50)			2390(2.21)
(1×1)	2820(2.59)	2690(2.47)			1970(1.81)
(2×1)	1550(1.42)		1590(1.47)	1610(1.49)	1910(1.76)

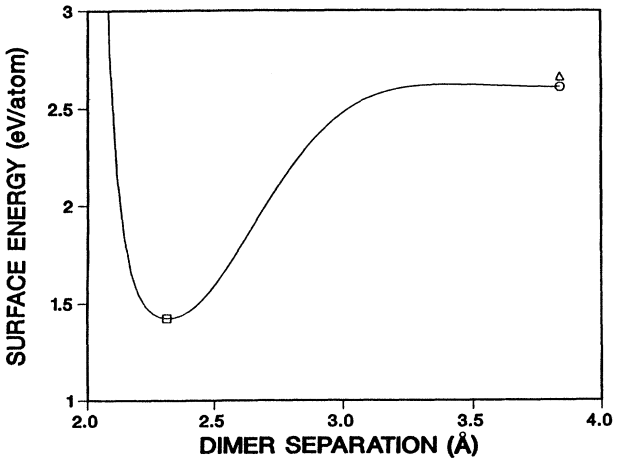

FIG. 7. Total energy vs symmetric-dimer-atomic spacing. For each spacing, the total energy is minimized by relaxing atomic positions in the top five atomic layers. The triangle indicates the surface energy of the (1×1) unrelaxed surface, which is 2850 erg/cm^2 (2.63 eV/atom). The open circle shows the surface energy of the planar-relaxed (1×1) surface, which is 2820 erg/cm^2 (2.59 eV/atom). The minimum in the energy curve is indicated by the open box, which is the (2×1) relaxed surface at a surface energy of 1550 erg/cm^2 (1.42 eV/atom). The dimer interatomic separation at the minimum is 2.31 Å, slightly smaller than the bulk nearest-neighbor distance of 2.35 Å. We found that if we removed the symmetric dimer constraint the equilibrium (2×1) energy and spacing was unchanged.

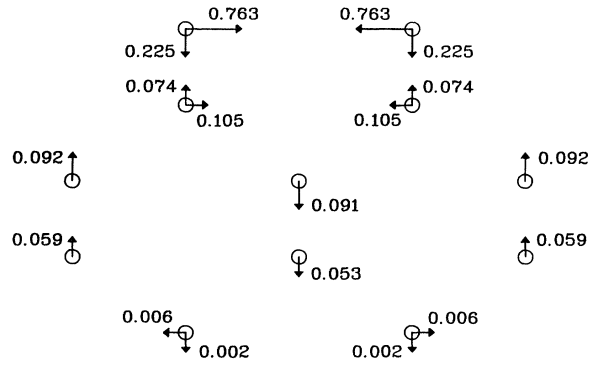

FIG. 8. Side view of atomic displacements for (2×1) reconstruction of Si(100). The displacements are in Å.

tains one relatively deep well.

The energy of the (2×1) reconstructed surface computed via ECT is compared with the results of other calculations in Table X. The surface energies from Refs. 58 and 59 were obtained by subtracting the dimer reconstruction energies reported in those references from the ideal surface energy reported in Ref. 24. One can see that there is good agreement between the ECT energy for the (2×1) surface and the first-principles values of Ref. 58 and 59. Again the equivalent-crystal method exhibits relatively high accuracy, despite being considerably simpler than the first-principles methods. As mentioned earlier, the method of Ref. 16 has an ease of application similar to ECT. The (2×1) energy prediction from Ref. 16 shown in Table X is somewhat larger than all of the other predictions.

Next let us examine the relative contributions of σ_1, σ_2, σ_3, and σ_4 to the surface energy σ of reconstructed Si(100). The results are listed in Table XI. These can be compared with the planar relaxation results for metals listed in Table IV. In the cases of planar relaxations of metals discussed earlier, we found that contributions to the surface energy due to bond-length, face diagonal, and bond-angle anisotropies were quite small, although bond-length anisotropy contributed importantly to equilibrium interplanar spacings. We found in the case of Si reconstruction that bond-length anisotropy was again important to the computation of equilibrium interatomic separations, even though σ_2 was relatively small. This, as in metals, is primarily due to a large force contribution in compression from bond-length anisotropy, which keeps equilibrium bond lengths close to bulk nearest-neighbor distances and thereby keeps σ_2 relatively small. Also as in the case of metals, σ_1 provides the largest component of the surface energy. One obvious difference between Tables IV and XI is the much larger contribution of the bond-angle anisotropy term σ_3 and the face diagonal term σ_4 in the case of Si. Generally bond-angle effects are thought to be more important in semiconductors than

TABLE XI. Surface energy components of Si(100) after reconstruction in erg/cm^2. The values in parentheses are in eV per surface atom. Layer 1 is the surface atomic layer.

Layer	σ_1	σ_2	σ_3	σ_4	Layer sum
1	1125.1(1.035)	13.0(0.012)	0.0(0.0)	0.0(0.0)	1138.2(1.045)
2	0.16(0.0)	13.9(0.013)	282.1(0.260)	36.6(0.034)	332.8(0.306)
3	14.9(0.0137)	7.8(0.0073)	24.3(0.023)	1.9(0.0018)	49.1(0.046)
4	5.8(0.005)	5.8(0.005)	6.1(0.006)	0.013(0.0)	17.7(0.016)
5	0.11(0.0)	8.35(0.008)	0.23(0.0)	0.57(0.0)	9.3(0.009)
6	0.0(0.0)	0.0(0.0)	0.0(0.0)	0.0(0.0)	0.08(0.0)
7	0.0(0.0)	0.0(0.0)	0.0(0.0)	0.0(0.0)	0.0(0.0)
Totals	1146.2(1.05)	49.0(0.045)	311.8(0.287)	38.9(0.036)	1545.8(1.422)

TABLE XII. Calculated atomic displacements for reconstruction of Si(100). The ideal Si(100) surface undergoes a symmetric-dimer reconstruction to form the (2×1) surface. Displacements are in Å. See Fig. 8 for a plot of displacements.

Layer	ECT		Ref. 60	
	x	z	x	z
1	+0.763	−0.225	+0.695	−0.092
2	+0.105	+0.074	+0.119	+0.005
3	+0.0	+0.092	+0.0	+0.130
	+0.0	−0.091	+0.0	−0.130
4	+0.0	+0.059	+0.0	+0.076
	+0.0	−0.053	+0.0	−0.076
5	−0.006	−0.002	−0.033	+0.0
	−0.006	−0.002		

in metals, so this is not surprising. After all, the diamond structure of these semiconductors is due in part to directional bonding. As there are $\frac{1}{3}$ as many nearest neighbors in the diamond structure as in the fcc structure, in a sense there is more room in the diamond structure for reconstructions that could involve relatively larger changes in bond angles, leading to relatively larger σ_3 and σ_4 contributions. One must reserve judgment on comparisons of metal and semiconductor surface energetics until similar calculations have been carried out for a metal where there is surface reconstruction. For such metallic reconstructions, σ_3 may be significant.

Another potential difference between Si(100) reconstruction and the planar relaxations of metals is seen by comparing Tables XI and VI. In Table VI only Δd_{12} and Δd_{23} values are listed because movements of deeper layers are much smaller. It is clear from Table XI, however, that the surface disturbance runs somewhat deeper for Si(100) reconstruction. Table XII exhibits computed atomic displacements for Si(100). The same displacements are plotted in Fig. 8. The coordinate z is taken perpendicular to the surface. These are compared in Table XII with the first-principles computations of Ref. 27. The agreement is reasonable, despite the relative simplicity of our method.

IV. SUMMARY

Our goal has been to provide a method with which physicists and materials scientists might treat real material defects and surfaces accurately at the atomic level. The method has to be sufficiently simple to apply that surfaces and other low-symmetry defects often encountered can be treated with modern computers. The simplicity offers the advantage that the physics becomes transparent, but it is difficult to have both simplicity and accuracy. We also would like to have a method which treats both semiconductors and metals on the same footing, so that differences in properties of these classes of materials are not method dependent.

Our approach has been to treat the solid defect as a perturbation on a single crystal. This provides us with an exact framework to guide our approximations. To minimize the size of the perturbation and hence the number of terms in the perturbation series required, we carry out the perturbation on a crystal whose lattice constant is different from that of the ground-state crystal. In fact we adjust that lattice constant until the perturbation sums to zero. In that case the energy of an atom in the crystal is equal to the energy of the defect atom it represents. We call the crystal at that lattice constant an *equivalent crystal*. The energy of the crystal as a function of lattice constant is analytically represented by the universal energy relation. This leads to a particularly simple method, involving one equation and one unknown. The one unknown is the equivalent-crystal lattice constant and the one equation is the perturbation sum equal to zero.

The exact perturbation sum is in fact quite complicated, however. We simplify it into four types of terms. The first term depends only on average neighbor distances, and so is akin to a "volume" term. The second term depends on bond-length anisotropies, while the third term is a function of bond-angle anisotropies. The fourth term is a function of face diagonal anisotropies. These four types of terms are simple and they display the physics readily.

We carried out a number of applications of the method to metallic and semiconductor surfaces and defects. Surfaces are a severe test of a method based on perturbation of a single crystal. Surface and defect formation energies and atomic locations are predicted accurately on comparison with first-principles and experimental results.

Thus this method appears to be quite promising. A number of other applications are in progress, including extensions of the method to treat both alloys and impurities.

ACKNOWLEDGMENTS

The authors would like to acknowledge with thanks useful conversations with Dr. Jan Herbst, Dr. John Larson, Dr. Walter Kohn, Dr. Stephen Harris, Dr. David Srolovitz, and Dr. Tao Hong.

APPENDIX

It is useful to have an analytic expression for the force on an atom as a function of the coordinates of its neighbors. This facilitates molecular-dynamics calculations and also can guide the search for energy minima in static applications. The force $\mathbf{F}_m$ on atom m is

$$\mathbf{F}_m = -\nabla_m \varepsilon \ , \tag{A1}$$

where ε is given by Eqs. (5) and (20). In the following, we provide the x component of the force, F_m^x. F_m^y and F_m^z are obtained by replacing x_m with y_m or z_m, respectively,

$$F_m^x = -\Delta E \sum_i \left[\partial f_1(i)/\partial x_m + \partial f_2(i)/\partial x_m + \sum_{j,k} \partial f_3(i,j,k)/\partial x_m + \sum_{p,q} \partial f_4(i,p,q)/\partial x_m \right] , \tag{A2}$$

where

$$\partial f_1(i)/\partial x_m = a_1^*(i) e^{-a_1^*(i)} \partial a_1^*(i)/\partial x_m \ , \tag{A3}$$

$$\partial f_2(i)/\partial x_m = a_2^*(i) e^{-a_2^*(i)} \partial a_2^*(i)/\partial x_m \ , \tag{A4}$$

$$\partial f_3(i,j,k)/\partial x_m = a_3^*(i,j,k) e^{-a_3^*(i,j,k)} \times \partial a_3^*(i,j,k)/\partial x_m \ , \tag{A5}$$

and

$$\partial f_4(i,p,q)/\partial x_m = a_4^*(i,p,q) e^{-a_4^*(i,p,q)} \times \partial a_4^*(i,p,q)/\partial x_m \ . \tag{A6}$$

Equations (A3)–(A6) follow immediately from Eq. (21). We are assuming a metal for the bond-length anisotropy term, Eq. (A4). The result for a semiconductor follows similarly. Note that each force term is zero at equilibrium [$a_1^*(i)=0$, $a_2^*(i)=0$, $a_3^*(i,j,k)=0$, and $a_4^*(i,p,q)=0$]. It remains to specify the partial derivatives on the right-hand side of Eqs. (A3)–(A6). These follow from Eq. (22),

$$\partial a^*/\partial x_m = (1/cl)\partial R_{ec}/\partial x \ , \tag{A7}$$

and Eqs. (26), (30), (39), and (40). First, we compute $\partial a_1^*(i)/\partial x_m$ from Eq. (26).

For $i=m$,

$$\partial a_1^*(i)/\partial x_m = (1/clN_1) \times \sum_k [g(R_k)/g(R_{ec})](x_i - x_k)/R_k \ , \tag{A8}$$

and for $i \neq m$ (but a nearest neighbor),

$$\partial a_1^*(i)/\partial x_m = (1/clN_1)[g(R_m)/g(R_{ec})] \times (x_m - x_i)/R_m \ , \tag{A9}$$

where

$$g(R) = R^{p-1} e^{-\alpha R}(p - \alpha R) \ , \tag{A10}$$

and R_{ec} is the solution of Eq. (26) for atom i. Equations (A8) and (A9) follow from differentiating Eq. (26) with respect to x_m, keeping only nearest neighbors in this approximation.

If $m \neq i$ or a nearest neighbor to i, then

$$\partial a_2^*(i)/\partial x_m = 0 \ . \tag{A11}$$

Next, we compute $\partial a_2^*(i)/\partial x_m$ from Eq. (30).

For $i=m$,

$$\partial a_2^*(m)/\partial x_m = [A_2 R_0^p/cN_1 lg(R_{ec})] \times \sum_j h(R_j)(x_m - x_j) \ , \tag{A12}$$

where

$$h(R) = e^{-\beta(R-R_0)}[1-\beta(R-R_0)]/R \ . \tag{A13}$$

For $i \neq m$, but m a nearest neighbor to i,

$$\partial a_2^*(i)/\partial x_m = [A_2 R_0^p/cN_1 lg(R_{ec})] h(R_m)(x_m - x_i) \ . \tag{A14}$$

For Eqs. (A12) and (A14), R_{ec} is the solution of Eq. (30).

Next, we compute $\partial a_3^*(i,p,q)/\partial x_m$ from Eq. (39):

$$\partial a_3^*(i,j,k)/\partial x_m = -[A_3 R_0^p/cN_1 lg(R_{ec})] \times (d_1 \cot\theta_{jk} - d_2)\partial \cos\theta_{jk}/\partial x_m \ , \tag{A15}$$

where d_1, d_2 are $-\frac{1}{3}, -2\sqrt{2}/3$ for bcc; $0, -1$ for fcc; and $\frac{1}{3}, -2\sqrt{2}/3$ for diamond structures, and R_{ec} is the solution of Eq. (39).

For $i=m$,

$$\partial \cos\theta_{jk}/\partial x_m = (1/R_j R_k)[2x_i - (x_j + x_k)] + [(x_k - x_i)/R_k^2 + (x_j - x_i)/R_j^2] \times \cos\theta_{jk} \ . \tag{A16}$$

For $j=m$,

$$\partial \cos\theta_{jk}/\partial x_m = (1/R_j R_k)(x_k - x_i) + [(x_i - x_j)/R_j^2]\cos\theta_{jk} \ , \tag{A17}$$

and similarly for $k=m$.

If $m \neq i$, j, or k, then

$$\partial a_3^*(i,j,k)/\partial x_m = 0 \ . \tag{A18}$$

Finally, we compute $\partial a_4^*(i,p,q)/\partial x_m$ from Eq. (40). This force is nonzero only when m is nearest neighbor to atom i. Thus, e.g., it is zero when $m=i$:

$$\partial a_4^*(i,p,q)/\partial x_m = -[A_4 R_0^p/dcN_1 lg(R_{ec})] \times (x_m - x_k)/|\mathbf{R}_m - \mathbf{R}_k| \ , \tag{A19}$$

where atom k is at an opposite corner of a cube face from atom m and R_{ec} is a solution of Eq. (40).

[1] *Atomistic Simulation of Materials Beyond Pair Potentials,* edited by V. Vitek and D. J. Srolovitz (Plenum, New York, 1989).

[2] M. S. Daw, Phys. Rev. B **39**, 7441 (1989), and references cited therein; M. S. Daw and M. I. Baskes, *ibid.* **29**, 6443 (1984).

[3] The *N*-body-potential method is closely related to the embedded-atom method. See M. W. Finnis and J. E. Sinclair, Philos. Mag. A **50**, 45 (1984).

[4] Preliminary discussions and applications of this method can be found in J. R. Smith and Amitava Banerjea, Phys. Rev. Lett. **59**, 2451 (1987), and in the following three references.

[5] J. R. Smith and A. Banerjea, Phys. Rev. B **37**, 10411 (1988).

[6] J. R. Smith, T. A. Perry, and A. Banerjea, in *Atomistic Simulation of Materials Beyond Pair Potentials* (Ref. 1), p. 279.

[7] J. R. Smith, G. Bozzolo, A. Banerjea, and J. Ferrante, Phys. Rev. Lett. **63**, 1269 (1989).

[8] W. Kohn and L. J. Sham, Phys. Rev. **140**, A1113 (1965).

[9] K. W. Jacobsen, J. K. Norskov, and M. J. Puska, Phys. Rev. B **35**, 7423 (1987), and references cited therein; see, in particu-

lar, M. J. Stott and E. Zaremba, *ibid.* **22**, 1564 (1980).
[10]J. H. Rose, J. Ferrante, and J. R. Smith, Phys. Rev. Lett. **47**, 675 (1981).
[11]For a review, see A. Banerjea and J. R. Smith, Phys. Rev. B **37**, 6632 (1988), and references cited therein. See also P. Vinet, J. H. Rose, J. Ferrante, and J. R. Smith, J. Phys. Condens. Matter **1**, 1941 (1989).
[12]J. H. Rose, J. R. Smith, and J. Ferrante, Phys. Rev. B **28**, 1835 (1983).
[13]S. M. Foiles, Phys. Rev. B **32**, 7685 (1985).
[14]R. A. Johnson, Phys. Rev. B **39**, 12 554 (1989).
[15]J. Tersoff, Phys. Rev. B **37**, 6991 (1988).
[16]M. I. Baskes, J. S. Nelson, and A. F. Wright, Phys. Rev. B **40**, 6085 (1989).
[17]B. W. Dodson, Phys. Rev. B **35**, 2795 (1987).
[18]John R. Smith and John Ferrante, Phys. Rev. B **34**, 2238 (1986); E. G. Brovman and Yu. Kagan, Zh. Eksp. Teor. Fiz. **57**, 1329 (1969) [Sov. Phys. JETP **30**, 721 (1970)]; V. Heine and D. Weaire, in *Solid State Physics,* edited by H. Ehrenreich, F. Seitz, and D. Turnbull (Academic, New York, 1970), Vol. 24, especially p. 277.
[19]John A. Moriarty, Phys. Rev. B **42**, 1609 (1990).
[20]Guillermo Bozzolo, John Ferrante, and John R. Smith (unpublished).
[21]J. R. Smith, F. J. Arlinghaus, and J. G. Gay, Phys. Rev. B **26**, 1071 (1982).
[22]H. J. Wollenberger, in *Physical Metallurgy,* 3rd ed., edited by R. W. Cahn and P. Haasen (North-Holland, New York, 1983), Part II, Chap. 17. The value for Pd was taken from S. M. Foiles, M. I. Baskes, and M. S. Daw, Phys. Rev. B **33**, 7983 (1986).
[23]Y. Ohta, M. W. Finnis, D. G. Pettifor, and A. P. Sutton, J. Phys. F **17**, L273 (1987).
[24]M. T. Yin and Marvin L. Cohen, Phys. Rev. B **24**, 2303 (1981).
[25]See, e.g., Y. K. Syrkin and M. E. Dyatkina, *Structure of Molecules and the Chemical Bond* (Interscience, New York, 1950), pp. 237–261.
[26]A. Antonelli and J. Bernholc, Phys. Rev. B **40**, 10 643 (1989), and references cited therein.
[27]S. Raimes, *The Wave Mechanics of Electronics in Metals* (North-Holland, Amsterdam, 1967), p. 305.
[28]V. L. Moruzzi, J. F. Janak, and A. R. Williams, *Calculated Electronic Properties of Metals* (Pergamon, New York, 1978), p. 26, Fig. 3.2.
[29]John R. Smith, Phys. Rev. **181**, 522 (1969), Table III.
[30]Leonard Kleinman, Phys. Rev. **128**, 2614 (1962).
[31]Walter A. Harrison, *Electronic Structure and the Properties of Solids* (Freeman, San Francisco, 1980), p. 197.
[32]C. Kittel, *Introduction to Solid State Physics,* 4th ed. (Wiley, New York, 1971).
[33]G. Simmons and H. Wang, *Single Crystal Elastic Constants and Calculated Aggregate Properties: A Handbook,* 2nd ed. (Wiley, New York, 1971).
[34]S. M. Foiles, M. I. Baskes, and M. S. Daw, Phys. Rev. B **33**, 7893 (1986). The EAM results in Table VI for Al(110) and Ni(110) were computed by S. P. Chen, D. J. Srolovitz, and A. F. Voter, J. Mater. Res. **4**, 62 (1989).
[35]J. A. Appelbaum and D. R. Hamann, Solid State Commun. **27**, 881 (1978).
[36]J. G. Gay, J. R. Smith, Roy Richter, F. J. Arlinghaus, and R. H. Wagoner, J. Vac. Sci. Technol. A **2**, 931 (1984); J. R. Smith, J. Ferrante, P. Vinet, J. G. Gay, Roy Richter, and J. H. Rose, in *Chemistry and Physics of Fracture,* edited by R. H. Jones and R. M. Latanision (Nijhoff, Hingham, MA, 1987).
[37]K. M. Ho and K. P. Bohnen, Phys. Rev. B **32**, 3446 (1985).
[38]C. L. Fu, S. Ohnishi, H. J. F. Jansen, and A. J. Freeman, Phys. Rev. B **31**, 1168 (1985).
[39]D. L. Adams, H. B. Nielsen, J. N. Andersen, I. Stensgaard, R. Feidenhan'sl, and J. E. Sørensen, Phys. Rev. Lett. **49**, 669 (1982).
[40]M. Copel, T. Gustafsson, W. R. Graham, and S. M. Yalisove, Phys. Rev. B **33**, 8110 (1986).
[41]R. Mayer, C. Zhang, K. G. Lynn, W. E. Frieze, F. Jona, and P. M. Marcus, Phys. Rev. B **35**, 3102 (1987).
[42]H. L. Davis and J. R. Noonan, Surf. Sci. **126**, 245 (1983).
[43]S. A. Lindgren, L. Wallden, J. Rundgren, and P. Westrin, Phys. Rev. B **29**, 576 (1984).
[44]Y. Kuk and L. C. Feldman, Phys. Rev. B **30**, 5811 (1984).
[45]D. L. Adams, L. E. Petersen, and C. S. Sorensen, J. Phys. C **18**, 1753 (1985).
[46]S. M. Yalisove, W. R. Graham, E. D. Adams, M. Copel, and T. Gustafsson, Surf. Sci. **171**, 400 (1986).
[47]J. W. M. Frenken, J. F. van der Veen, and G. Allan, Phys. Rev. Lett. **51**, 1876 (1983).
[48]J. E. Demuth, P. M. Marcus, and D. W. Jepsen, Phys. Rev. B **11**, 1460 (1975).
[49]J. N. Andersen, H. B. Nielsen, L. Petersen, and D. L. Adams, J. Phys. C **17**, 173 (1984).
[50]J. R. Noonan and H. L. Davis, Phys. Rev. B **29**, 4349 (1984).
[51]H. B. Nielsen and D. L. Adams, J. Phys. C **15**, 615 (1982).
[52]H. d'Amour, W. Denner, H. Schulz, and M. Cardona, J. Appl. Crystallogr. **15**, 148 (1982).
[53]C. S. G. Cousins, L. Gerward, K. Nielsen, J. Staun Olsen, B. Selsmark, B. J. Sheldon, and G. E. Webster, J. Phys. C **15**, L651 (1982).
[54]O. H. Nielsen and Richard M. Martin, Phys. Rev. B **32**, 3792 (1985).
[55]C. S. G. Cousins, J. Phys. C **15**, 1857 (1982).
[56]John E. Northrup, J. Ihm, and Marvin L. Cohen, Phys. Rev. Lett. **47**, 1910 (1981).
[57]R. J. Hamers, R. M. Tromp, and J. E. Demuth, Phys. Rev. B **34**, 5343 (1986), and references cited therein.
[58]K. C. Pandey, in *Proceedings of the Seventh International Conference on the Physics of Semiconductors,* edited by D. J. Chadi and W. A. Harrison (Springer-Verlag, New York, 1985), p. 55.
[59]N. Roberts and R. J. Needs, J. Phys. Condens. Matter **1**, 3139 (1989).
[60]Joel A. Appelbaum and D. R. Hamann, Surf. Sci. **74**, 21 (1978).